IL6ST–induced muscarinic receptor opens goblet cell associated antigen passages to suppress alcoholic liver disease

Michael Karin (karinoffice@ucsd.edu)
University of California, San Diego https://orcid.org/0000-0002-2758-6473
Cristina Llorente
University of California San Diego https://orcid.org/0000-0001-8135-9186
Ryan Bruellman
Université Catholique de Louvain
Noemí Cabré
University of California, San Diego
Rocío Brea
University of California, San Diego
Nuria Pell
University of California, San Diego
Luca Maccioni
Université Catholique de Louvain
Ameera Alghafri
University of California, San Diego
Rongrong Zhou
Xiangya Hospital, Central South University, and Key Laboratory of Viral Hepatitis
Bei Gao
University of California, San Diego
Yi Duan
University of California, San Diego
Junlai Liu
University of California, San Diego
Koji Taniguchi
Keio University School of Medicine and Hokkaido University
Rodney Newberry
Washington University in St. Louis, School of Medicine https://orcid.org/0000-0002-4152-5191
Derrick Fouts
J. Craig Venter Institute https://orcid.org/0000-0003-4323-7668
David Brenner

University of California, San Diego

Peter Starkel

Cliniques Universitaires St. Luc https://orcid.org/0000-0003-2938-4442

Bernd Schnabl

VA San Diego Healthcare System

Biological Sciences - Article

Keywords: alcoholic liver disease, liver damage

Posted Date: April 3rd, 2021

DOI: https://doi.org/10.21203/rs.3.rs-366644/v1

IL6ST–induced muscarinic receptor opens goblet cell associated antigen passages to suppress alcoholic liver disease

Cristina Llorente[1], Ryan Bruellman[1], Noemí Cabré[1], Rocío Brea[1], Nuria Pell[1], Luca Maccioni[2], Ameera Alghafri[1], Rongrong Zhou[1,3], Bei Gao[1], Yi Duan[1], Junlai Liu[4], Koji Taniguchi[4, 5, 6], Rodney D. Newberry[7], Derrick E. Fouts[8], David A. Brenner[1], Peter Stärkel[2,9], Michael Karin[4]*, Bernd Schnabl[1,10]*

[1]Department of Medicine, University of California San Diego, La Jolla, CA, USA;[2]Institute of Experimental and Clinical Research, Laboratory of Hepato-gastroenterology, UCLouvain, Université Catholique de Louvain, Brussels, Belgium;[3]Department of Infectious Diseases, Xiangya Hospital, Central South University, and Key Laboratory of Viral Hepatitis, Hunan, Changsha, China;[4]Laboratory of Gene Regulation and Signal Transduction, Departments of Pharmacology and Pathology, University of California San Diego, La Jolla, CA, USA; [5]Department of Microbiology and Immunology, Keio University School of Medicine, Shinjuku-ku, Tokyo, Japan;[6]Department of Pathology, Faculty of Medicine and Graduate School of Medicine, Hokkaido University, Sapporo, Hokkaido, Japan;[7]Department of Internal Medicine, Washington University School of Medicine, St. Louis, Missouri, USA; [8]J. Craig Venter Institute, Rockville, MD, USA;[9]Department of Hepato-gastroenterology, Cliniques Universitaires Saint-Luc, Brussels, Belgium;[10]Department of Medicine, VA San Diego Healthcare System, San Diego, CA, USA

Abbreviations: ACh, acetylcholine; ALD, alcoholic liver disease; ALT, alanine amino-transferase; AMP, antimicrobial peptides; ANOVA, analysis of variance; APCs; antigen presenting cells, AUD, alcohol use disorder; BHI broth, brain heart infusion broth; CD, cluster of differentiation; CFU, colony forming unit; CK18, cytokeratin 18; Cxcl, chemokine (C-X-C motif); CX3CR1, C-X3-C Motif Chemokine Receptor; DC, dendritic cell; *E. faecalis; Enterococcus faecalis*; EGFP, green fluorescent protein; FOXP3, forkhead box P3; GAP, goblet cell associated antigen passage; GC, goblet cell; H&E, hematoxylin and eosin; IEC, intestinal epithelial cells; IL, interleukin; ILC, innate lymphoid cell; IL6ST, IL-6 signal transducer; LP, lamina propria; mAChR, muscarinic ACh receptor; MHC, major histocompatibility class; MLN, mesenteric lymph node; ORO, oil red O; OTU, operational taxonomic unit; PAM, positive allosteric modulator; PAS, Periodic Acid/Schiff; PBS, phosphate-buffered saline; PCoA, principal coordinate analysis; PEA, phenylethyl alcohol; PMA, phorbol 12-myristate 13-acetate; qPCR, quantitative polymerase chain reaction; Reg3, C-type regenerating islet derived-3; rRNA, ribosomal RNA; s.e.m., standard error of the mean; TMR, tetramethylrhodamine; TLR; Toll-like receptor; Treg, T regulatory cell; WT, wild type.

Summary

Alcohol consumption is the seventh leading risk factor for death worldwide [1] and alcoholic liver disease (ALD) is the major cause of liver transplantation in the West [2]. Alcohol metabolites can directly damage the liver, but the gut-liver axis also plays an important role in ALD pathogenesis, acting through complex and obscure mechanisms. Although alcohol intake is associated with increased intestinal permeability [3], it is not clear how the intestinal immune system affects liver disease. Paradoxically, we found that chronic alcohol use increases intestinal goblet cell (GC) number and mucin production in patients and mice. This, however, comes with the expense of GC associated antigen passages (GAPs) closure and defective delivery of luminal antigens and bacteria to lamina propria (LP) antigen presenting cells (APCs). IL-6 is one of several cytokines elevated in ALD that affects the liver and the intestine [4]. Although IL-6 expression correlates with disease severity [5], IL-6 also exerts barrier protective effects [6]. We now show that GAPs are controlled by intestinal IL-6 signal transducer (IL6ST/gp130). Although mice that express constitutively active gp130 in intestinal epithelial cells (IEC; *gp130*$^{Act/IEC}$ mice) have fewer GCs [7], they are ALD resistant due to increased GAP formation, which enhances the generation of tolerogenic LP-APCs and production of IL-22 by type-3 innate lymphoid cells (ILC3s). GAP opening induces an intestinal C-type regenerating islet derived-3 (Reg3) lectin-mediated antibacterial defense, reducing bacterial translocation to the liver and preventing alcoholic steatohepatitis. gp130 signaling exerted its protective effects via muscarinic acetylcholine (ACh) receptor 4 (mAChR4), whose GC expression was induced by IL-6. Based on these findings, we developed a new therapeutic approach, administering a mAChR4 positive allosteric modulator (PAM) to stimulate intestinal GAP formation, thereby increasing tolerogenic LP-APCs and Reg3 expression, to prevent microbial translocation and protect mice from alcoholic steatohepatitis.

Our results show that IL6ST signaling modulates intestinal immunity through mAChR4. GAP induction by mAChR4 PAMs is a promising strategy for enhancing intestinal immune tolerance and interception in ALD and other diseases linked to uncontrolled microbial translocation.

Main

Alcohol consumption is the seventh leading risk factor for death worldwide [1], and ALD is the major cause of liver transplantation in the West [2]. There is no treatment for ALD except for abstinence. Chronic alcohol abuse is associated with increased intestinal permeability, dysbiosis and translocation of viable bacteria, such as *Enterococcus faecalis* (*E. faecalis*), to the liver, enhancing inflammation and accelerating ALD progression [8,9]. Intestinal immune-microbiome interactions are altered during ALD [10]. Such findings suggest that the intestinal immune system may control ALD pathogenesis. To test this hypothesis and elucidate the underlying mechanisms we investigated how chronic alcohol exposure affects the intestinal immune system and bacterial translocation to the liver. The findings described below are of relevance to other diseases associated with loss of intestinal barrier integrity.

Chronic alcohol abuse alters GC biology in mice and humans

GCs secrete mucins which coat the IEC apical surface and prevent microbial adhesion and translocation [11]. Paradoxically, chronic ethanol administration increased production of mucin-2 (Muc2), the most abundant intestinal mucin [12], and the number of small intestine mucin secreting GCs in mice (Fig. 1a–1b) and patients with alcohol use disorder (AUD) (Fig. 1c–1d). Small intestinal GCs deliver luminal antigens and bacteria to LP-APCs through GAPs, thereby inducing adaptive immune responses [13,14]. GAPs are formed immediately after mucin is secreted into the intestinal lumen [13]. We observed that the number of GAPs, identified as dextran-filled columns traversing Muc2 positive nucleated cells, was reduced following chronic ethanol feeding (Fig. 1e–1f). Small intestinal GAPs are dynamic, and they open in response to ACh, which engages muscarinic mAChR4 on GCs [15,16]. The observed reduction in GAP formation after ethanol

exposure could be related to reduced expression of *Chrm4,* the gene for mAChR4 (Fig. 1g). When we gavaged mice with enhanced green fluorescent protein (EGFP)-*E. faecalis*, we found colocalization of bacteria with Muc2 inside GCs (Fig. 1h) and with dextran-filled GAP columns (Fig. 1i), suggesting that bacteria are sampled by GCs. These results indicate that chronic alcohol use increases protective mucin production, which paradoxically comes with the expense of GAP closure.

IL6ST-mediated induction of GAPs prevents ethanol-induced liver disease

IL-6 is one of several cytokines elevated in ALD that affects the liver and the intestine [4]. Although IL-6 correlates with liver disease severity [5], it also exerts important barrier protective effects [6]. Of note, IL-6 treatment induced mAChR4 expression in small intestinal organoids (Fig. 2a–2c). Previously, we showed that IL-6 signaling promotes intestinal stem cell survival and proliferation by activating STAT3 and YAP and that *gp130*$^{Act/IEC}$ mice are resistant to mucosal erosion, despite having fewer GCs than wild type (WT) mice [7]. Remarkably, *gp130*$^{Act/IEC}$ mice were protected from ethanol-induced liver injury compared with WT littermates, as indicated by lower plasma alanine amino-transferase (ALT) (Fig. 2d) and reduced hepatic steatosis (Fig. 2e–2f) and inflammation (Fig. 2g–2h), while having fewer GCs and lower Muc2 expression in the small intestine (Fig. 2i–2j). Activation of gp130 in IEC did not affect food intake or intestinal ethanol absorption (Extended Data Fig. 1a–1b). In accordance with the *in vitro* experiments, *gp130*$^{Act/IEC}$ mice showed more GAPs in the small intestine (Fig. 2k–2l), expressed higher amounts of *Chrm4* mRNA (Fig. 2m) and mAChR4 protein in isolated GCs (Fig. 2n–2o and Extended Data Fig. 1c–1d). mAChR4 is expressed in IEC, GC, some LP immune cells and the enteric nervous system in the small intestine. mACR4 in GC was distributed above the nuclei and subjacent to the

secretory granules (Extended Data Fig. 1e). Ethanol-fed *gp130*$^{Act/IEC}$ mice were protected from intestinal bacterial overgrowth and showed a different fecal microbiota composition than WT littermates (Fig. 2p–2q). These results indicate that IL-6-gp130 regulation of intestinal GAPs impacts the development of ethanol-induced liver injury.

gp130$^{Act/IEC}$ mice show elevated tolerogenic APCs and antimicrobial defense

To study the consequences of GAP modulation, we characterized different subsets of CD11c$^+$, major histocompatibility class (MHC)II$^+$ LP-APCs [17]. Chronic ethanol-feeding in WT mice did not affect frequencies or numbers of CD11c$^+$, MHCII$^+$ APCs (Extended Data Fig. 2a–2c), but it reduced the frequencies of the CD103$^+$, CD11b$^+$, CX3CR1$^-$ dendritic cell (DC) subset (Fig. 3a), frequencies and numbers of CD103$^-$, CD11b$^+$, CX3CR1$^+$ APCs (Fig. 3b and Extended Data Fig. 2d), numbers of IL-23 expressing APC subsets (Fig. 3c), and IL-10 expressing APC subsets (Extended Data Fig. 2e). Correspondingly, ethanol decreased frequencies of ILC3s (CD3$^-$, RORγt$^+$) and IL-22 expressing ILC3s (Fig. 3d–3f).

Alcohol-induced suppression of the intestinal immune system was restored in *gp130*$^{Act/IEC}$ mice, which had increased frequencies and numbers of the tolerogenic APC subsets (CD103$^+$, CD11b$^+$, CX3CR1$^-$ and CD103$^-$, CD11b$^+$, CX3CR1$^+$) (Fig. 3a–3b and Extended Data Fig. 2d) and higher numbers of IL-23 and IL-10 expressing APC subsets (Fig. 3c and Extended Data Fig. 2e). Frequencies of ILC3s (CD3$^-$, ROR$_\gamma$t$^+$) were also increased in ethanol-fed *gp130*$^{Act/IEC}$ mice along with the number of IL-22 expressing ILC3s (Fig. 3d–3f). As a consequence, the Reg3g and Reg3b antimicrobial peptides were upregulated in *gp130*$^{Act/IEC}$ mice after ethanol administration (Fig. 3g–3i). As we have reported, increased Reg3 lectins might not only contribute to protection from bacterial overgrowth (Fig. 2p) but can also inhibit bacterial translocation [18]. Indeed, less viable

bacteria translocated from the intestine to mesenteric lymph nodes (MLNs) and liver of ethanol-fed *gp130*$^{Act/IEC}$ mice relative to WT mice (Fig. 3j–3k). Consistent with the increase in tolerogenic APC subsets, frequencies and numbers of T regulatory cells (Tregs) characterized as $CD4^+$, $CD25^+$, $FOXP3^+$ and levels of intestinal IL-10 were elevated in *gp130*$^{Act/IEC}$ mice after ethanol treatment (Extended Data Fig. 3a–3e). These results indicate that a specific tolerogenic APC-mediated intestinal adaptive immune response and antibacterial defenses might contribute to protection against ethanol-induced liver disease in mice.

_gp130_$^{Act/IEC}$ mice lose protection from ethanol-induced liver disease on mAChR4 antagonism

To determine whether gp130 exerts its protective effects via mAChR4-controlled GAP opening, mice were treated with the mAChR4 antagonist tropicamide. Tropicamide dissolved in the diet during the last 29 days of chronic ethanol feeding inhibited intestinal GAP formation (Fig. 3l–3m and Extended Data Fig. 4a) and made *gp130*$^{Act/IEC}$ mice lose protection from liver disease (Fig. 4n and Extended Data Fig. 4b), steatosis (Fig. 3o–3p and Extended Data Fig. 4c) and inflammation (Fig. 4q, Extended Data Fig. 4d–4e). Despite a tendency, tropicamide did not worsen the disease in WT mice, probably because ethanol already inhibited GAP formation in these mice (Fig. 1e–1g, Extended Data Fig. 4a). Tropicamide did not affect food intake or intestinal ethanol absorption (Extended Data Fig. 1a–1b). Tropicamide abrogated the increase in GAP-associated $CD103^+$, $CD11b^+$, $CX3CR1^-$ DCs and $CD103^-$, $CD11b^+$, $CX3CR1^+$ APCs, ILC3s and Tregs in ethanol-fed *gp130*$^{Act/IEC}$ mice (Fig. 3a–3b, 3d–3f, Extended Data Fig. 2d and Extended Data Fig. 3a–3c). Tropicamide treatment also reversed Reg3b and Reg3g protein induction in ethanol-fed *gp130*$^{Act/IEC}$ mice (Fig. 3r–3t), and significantly increased bacterial translocation to MLN and liver in ethanol-fed *gp130*$^{Act/IEC}$ mice (Fig. 3j–3k). Consistent with these results which suggest that IL-

6 induces mAChR4 whose activity is needed for IL-22 production and subsequent Reg3 induction, incubation of small intestinal organoids with IL-6 resulted in *Chrm4* but not *Reg3g* or *Reg3b* mRNA induction, whereas IL-22 induced *Reg3g* and *Reg3b* but not *Chrm4* mRNA (Extended Data Fig.4f–4h). These data demonstrate that intestinal gp130 activation exerts its liver protective effects via mAChR4-induced GAP formation.

Pharmacological manipulation of GAPs alleviates ethanol-induced liver injury

Based on these findings, we developed a new therapeutic approach, administering a mAChR4 PAM, VU0467154, to stimulate intestinal GAP formation. WT mice fed an ethanol containing diet for 10 weeks, were treated with VU0467154 during the last 29 days. VU0467154 has no gastrointestinal motility side effects and excellent oral bioavailability [19-21]. VU0467154 treatment abrogated ethanol-induced GAP closure (Fig. 4a–4b), and protected mice from ethanol–induced liver injury (Fig. 4c–4d), steatosis (Fig. 4e–4f) and inflammation (Fig. 4g). mAChR4 PAM treatment did not affect intestinal ethanol absorption, as pair-fed mice had similar blood alcohol levels (Extended Data Fig. 5a–5b). Frequencies of LP-APCs ($CD11c^+$, $MHCII^+$) and $CD103^+$ $CD11b^+$ DC populations in ethanol fed mice were increased by VU0467154 treatment (Fig. 4h–4k), which also induced intestinal Reg3g, Reg3b and IL-10 expression (Fig. 4l–4o) and prevented ethanol-mediated bacterial translocation to MLNs and liver (Fig. 4p–4q). Our results indicate that pharmacological manipulation of mAChR4 reduced ethanol-induced steatohepatitis.

Discussion

This study reveals a fine balance between physical barrier function and a protective intestinal immune response. Chronic alcohol increases intestinal mucin production, but this comes at the

expense of GAP closing and improper training of intestinal immunity. LP-APCs adjacent to GAPs induce specific protective immune responses that control intestinal homeostasis [13,15,16,22,23]. Regenerative responses are important after intestinal injury or microbial infection to maintain barrier integrity and prevent translocation of intestinal bacteria [24,25]. gp130 signaling stimulates regeneration and regulates differentiation of the gastrointestinal barrier through YAP and Notch activation [7,26-29]. Only very recently it was determined that inhibition of a dynamic neuroimmune circuit by activation of VIP receptor type 2 (VIPR2) in the intestine triggers IL-22 secretion by ILC3s and increases *Reg3g* mRNA in ileum [30]. Our findings add to the complex neuronal regulation of antibacterial defenses. Intestinal IL6ST/gp130 controls cholinergic signaling by upregulating mAChR4 on GCs to induce GAP formation (Extended Data Fig. 6). Therefore, IL6ST/gp130 signaling enhances the GC response to ACh released by GC-innervating parasympathetic neurons and possibly other cellular sources.

Ethanol therefore causes liver disease not only via direct toxic effects on liver cells, but also by suppressing the intestinal immune system and allowing enteric bacteria to translocate to the liver, underscoring the importance of the gut-liver axis for ALD pathogenesis. Consistent with this finding, pharmacological manipulation of mAChR4 with a PAM to induce small intestinal GAPs was associated with modulation of APCs, induction of Reg3 lectins, prevention of bacterial translocation and amelioration of ALD. Of note, whereas IL-6 induces mAChR4, IL-22 induces Reg3 lectins, suggesting that two cytokines act hierarchically and through different protective mechanisms, although both of them stimulate mucosal regeneration[31]. Interestingly, mAChR4 gene and protein expression are modulated in specific brain regions of AUD patients. The number of muscarinic receptors increases in several brain regions in the absence of alcohol during withdrawal [32]. Systemic administration of VU0467154 reduced ethanol seeking and consumption

in a rodent model [33]. We did not examine alcohol consumption in our mice, as they were pair-fed and received the same amount of ethanol-containing diet. Nevertheless, pharmacological manipulation of mAChR4 could be a potential approach for preventing not only ALD progression, but also for treating AUD. Targeted delivery of intestinal gp130 agonists to GCs and mAChR4 PAMs might be developed as a therapeutic agent for alcohol-related liver disease.

References

1 Collaborators, G. B. D. A. Alcohol use and burden for 195 countries and territories, 1990-2016: a systematic analysis for the Global Burden of Disease Study 2016. *Lancet* **392**, 1015-1035, doi:10.1016/S0140-6736(18)31310-2 (2018).

2 Lee, B. P., Vittinghoff, E., Dodge, J. L., Cullaro, G. & Terrault, N. A. National Trends and Long-term Outcomes of Liver Transplant for Alcohol-Associated Liver Disease in the United States. *JAMA Intern Med* **179**, 340-348, doi:10.1001/jamainternmed.2018.6536 2720757 [pii] (2019).

3 Lang, S. & Schnabl, B. Microbiota and Fatty Liver Disease-the Known, the Unknown, and the Future. *Cell Host Microbe* **28**, 233-244, doi:10.1016/j.chom.2020.07.007 (2020).

4 Hong, F. *et al.* Elevated interleukin-6 during ethanol consumption acts as a potential endogenous protective cytokine against ethanol-induced apoptosis in the liver: involvement of induction of Bcl-2 and Bcl-x(L) proteins. *Oncogene* **21**, 32-43, doi:10.1038/sj.onc.1205016 (2002).

5 Sheron, N., Bird, G., Goka, J., Alexander, G. & Williams, R. Elevated plasma interleukin-6 and increased severity and mortality in alcoholic hepatitis. *Clin Exp Immunol* **84**, 449-453 (1991).

6 Kuhn, K. A. *et al.* Bacteroidales recruit IL-6-producing intraepithelial lymphocytes in the colon to promote barrier integrity. *Mucosal Immunol* **11**, 357-368, doi:10.1038/mi.2017.55 (2018).

7 Taniguchi, K. *et al.* A gp130-Src-YAP module links inflammation to epithelial regeneration. *Nature* **519**, 57-62, doi:10.1038/nature14228 (2015).

8 Llorente, C. *et al.* Gastric acid suppression promotes alcoholic liver disease by inducing overgrowth of intestinal Enterococcus. *Nat Commun* **8**, 837, doi:10.1038/s41467-017-00796-x (2017).

9 Duan, Y. *et al.* Bacteriophage targeting of gut bacterium attenuates alcoholic liver disease. *Nature* **575**, 505-511, doi:10.1038/s41586-019-1742-x (2019).

10 Bruellman, R. & Llorente, C. A Perspective Of Intestinal Immune-Microbiome Interactions In Alcohol-Associated Liver Disease. *Int J Biol Sci* **17**, 307-327, doi:10.7150/ijbs.53589 (2021).

11 Velcich, A. *et al.* Colorectal cancer in mice genetically deficient in the mucin Muc2. *Science* **295**, 1726-1729, doi:10.1126/science.1069094 (2002).

12 Hartmann, P. *et al.* Deficiency of intestinal mucin-2 ameliorates experimental alcoholic liver disease in mice. *Hepatology* **58**, 108-119, doi:10.1002/hep.26321 (2013).

13 McDole, J. R. *et al.* Goblet cells deliver luminal antigen to CD103+ dendritic cells in the small intestine. *Nature* **483**, 345-349, doi:10.1038/nature10863 (2012).

14 Kulkarni, D. H. *et al.* Goblet cell associated antigen passages support the induction and maintenance of oral tolerance. *Mucosal Immunol* **13**, 271-282, doi:10.1038/s41385-019-0240-7 (2020).

15 Knoop, K. A., McDonald, K. G., McCrate, S., McDole, J. R. & Newberry, R. D. Microbial sensing by goblet cells controls immune surveillance of luminal antigens in the colon. *Mucosal Immunol* **8**, 198-210, doi:10.1038/mi.2014.58 (2015).

16 Knoop, K. A. *et al.* Antibiotics promote the sampling of luminal antigens and bacteria via colonic goblet cell associated antigen passages. *Gut Microbes* **8**, 400-411, doi:10.1080/19490976.2017.1299846 (2017).

17 Denning, T. L. *et al.* Functional specializations of intestinal dendritic cell and macrophage subsets that control Th17 and regulatory T cell responses are dependent on the T cell/APC ratio, source of mouse strain, and regional localization. *J Immunol* **187**, 733-747, doi:10.4049/jimmunol.1002701 (2011).
18 Wang, L. *et al.* Intestinal REG3 Lectins Protect against Alcoholic Steatohepatitis by Reducing Mucosa-Associated Microbiota and Preventing Bacterial Translocation. *Cell Host Microbe* **19**, 227-239, doi:10.1016/j.chom.2016.01.003 (2016).
19 Bubser, M. *et al.* Selective activation of M4 muscarinic acetylcholine receptors reverses MK-801-induced behavioral impairments and enhances associative learning in rodents. *ACS Chem Neurosci* **5**, 920-942, doi:10.1021/cn500128b (2014).
20 Pancani, T. *et al.* Allosteric activation of M4 muscarinic receptors improve behavioral and physiological alterations in early symptomatic YAC128 mice. *Proc Natl Acad Sci U S A* **112**, 14078-14083, doi:10.1073/pnas.1512812112 (2015).
21 Gould, R. W. *et al.* Cognitive enhancement and antipsychotic-like activity following repeated dosing with the selective M4 PAM VU0467154. *Neuropharmacology* **128**, 492-502, doi:10.1016/j.neuropharm.2017.07.013 (2018).
22 Knoop, K. A., McDonald, K. G., Kulkarni, D. H. & Newberry, R. D. Antibiotics promote inflammation through the translocation of native commensal colonic bacteria. *Gut* **65**, 1100-1109, doi:10.1136/gutjnl-2014-309059 (2016).
23 Kulkarni, D. H. *et al.* Goblet cell associated antigen passages are inhibited during Salmonella typhimurium infection to prevent pathogen dissemination and limit responses to dietary antigens. *Mucosal Immunol* **11**, 1103-1113, doi:10.1038/s41385-018-0007-6 (2018).
24 Medzhitov, R. Origin and physiological roles of inflammation. *Nature* **454**, 428-435, doi:10.1038/nature07201 (2008).
25 Ben-Neriah, Y. & Karin, M. Inflammation meets cancer, with NF-kappaB as the matchmaker. *Nature immunology* **12**, 715-723, doi:10.1038/ni.2060 (2011).
26 Gregorieff, A., Liu, Y., Inanlou, M. R., Khomchuk, Y. & Wrana, J. L. Yap-dependent reprogramming of Lgr5(+) stem cells drives intestinal regeneration and cancer. *Nature* **526**, 715-718, doi:10.1038/nature15382 (2015).
27 Yu, S. *et al.* Paneth Cell Multipotency Induced by Notch Activation following Injury. *Cell Stem Cell* **23**, 46-59 e45, doi:10.1016/j.stem.2018.05.002 (2018).
28 Todoric, J. *et al.* Fructose stimulated de novo lipogenesis is promoted by inflammation. *Nat Metab* **2**, 1034-1045, doi:10.1038/s42255-020-0261-2 (2020).
29 Romera-Hernandez, M. *et al.* Yap1-Driven Intestinal Repair Is Controlled by Group 3 Innate Lymphoid Cells. *Cell Rep* **30**, 37-45 e33, doi:10.1016/j.celrep.2019.11.115 (2020).
30 Talbot, J. *et al.* Feeding-dependent VIP neuron-ILC3 circuit regulates the intestinal barrier. *Nature* **579**, 575-580, doi:10.1038/s41586-020-2039-9 (2020).
31 Lindemans, C. A. *et al.* Interleukin-22 promotes intestinal-stem-cell-mediated epithelial regeneration. *Nature* **528**, 560-564, doi:10.1038/nature16460 (2015).
32 Nordberg, A. & Wahlström, G. Cholinergic mechanisms in physical dependence on barbiturates, ethanol and benzodiazepines. *Journal of Neural Transmission / General Section JNT* **88**, 199-221, doi:10.1007/BF01244733 (1992).
33 Walker, L. C. *et al.* Acetylcholine Muscarinic M4 Receptors as a Therapeutic Target for Alcohol Use Disorder: Converging Evidence From Humans and Rodents. *Biol Psychiatry* **88**, 898-909, doi:10.1016/j.biopsych.2020.02.019 (2020).

Figure 1

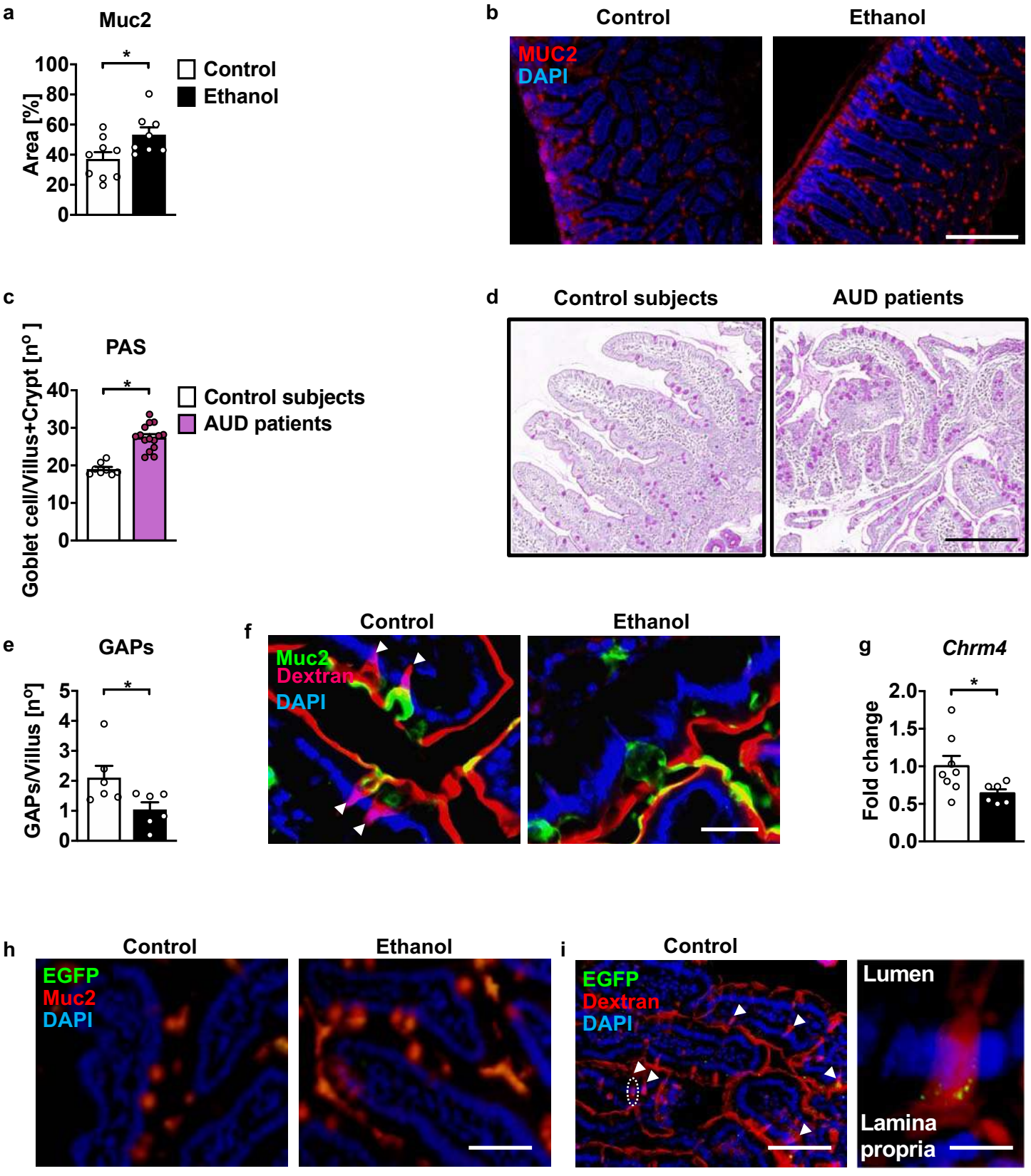
a
Muc2
Area [%]
100
80
60
40
20
0
*
Control
Ethanol
b
Control
Ethanol
MUC2
DAPI
c
PAS
Goblet cell/Villus+Crypt [n°]
40
30
20
10
0
*
Control subjects
AUD patients
d
Control subjects
AUD patients
e
GAPs
GAPs/Villus [n°]
5
4
3
2
1
0
*
f
Control
Ethanol
Muc2
Dextran
DAPI
g
Chrm4
Fold change
2.0
1.5
1.0
0.5
0.0
*
h
Control
Ethanol
EGFP
Muc2
DAPI
i
Control
EGFP
Dextran
DAPI
Lumen
Lamina propria

Figure 1. Chronic ethanol alters proximal intestinal GC in mice and humans. (a–b and e–i) C57BL/6 WT mice were fed control (n=6–9) or ethanol containing Lieber DeCarli diets (n=6–8) for 10 weeks. (a) Percentage of Muc2 positive stained area. (b) Representative sections of Muc2 (red) showing GCs and DAPI (blue) immunofluorescence staining. *Scale bar* = 250 μm. (c, d) Periodic Acid/Schiff (PAS) staining of paraffin-embedded small intestinal sections of duodenal biopsies from non-alcoholic controls (n=8) and patients with AUD (n=15). (c) Positive cells were enumerated in each villus and crypt. (d) Representative PAS-stained sections showing increased number of GCs in the duodenum of AUD patients as compared with controls. *Scale bar* = 100 μm. (e) To study GC GAP formation, a 2 cm loop in the small intestine was injected with tetramethylrhodamine (TMR) dextran and GAPs were counted as dextran-filled columns traversing the nucleated epithelium and positive for Muc2 staining. Number of GAPs per villus was quantified. (f) Representative sections stained with TMR-dextran (red) showing GAPs, Muc2 antibody (green) showing GCs and DAPI (blue) marking nuclei. *Scale bar* = 25 μm. (g) *Chrm4* mRNA was quantified by qPCR. (h) *E. faecalis* genetically modified with an EGFP vector (5 x 10^9 CFUs) were gavaged 9 h and 1 h before euthanasia (n=6). Representative sections stained with Muc2 antibody (red), EGFP (green) and DAPI (blue). Scale bar = 50 μm. (i) EGFP-*E. faecalis* (5 x 10^9 CFUs) were gavaged at 3 and 0.5 h before euthanasia (n=6). Representative section of EGFP (green), TMR-dextran (red) and DAPI (blue) stained intestinal sections. Left panel: *scale bar* = 100 μm, and right panel (amplification of the white discontinuous oval): *scale bar* = 12 μm. (f and i) Arrowheads indicate GAPs. *P* value was determined by two-sided unpaired Student *t* test or Mann-Whitney U-statistic test. Results are expressed as mean ± s.e.m. **P*<0.05.

Figure 2

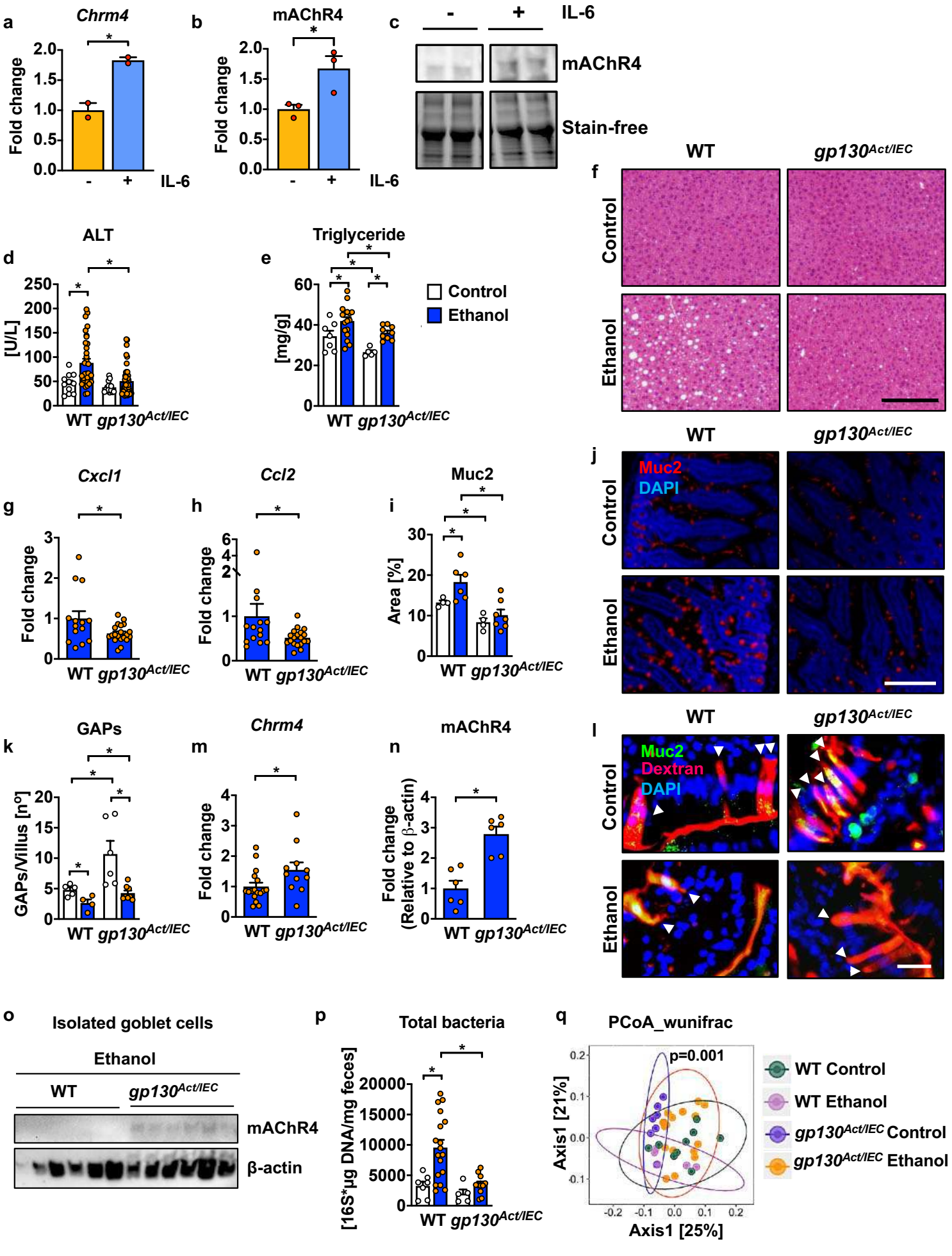
a
Chrm4
Fold change
IL-6
b
mAChR4
Fold change
IL-6
c
IL-6
mAChR4
Stain-free
d
ALT
[U/L]
WT gp130Act/IEC
e
Triglyceride
[mg/g]
Control
Ethanol
WT gp130Act/IEC
f
WT
gp130Act/IEC
Control
Ethanol
g
Cxcl1
Fold change
WT gp130Act/IEC
h
Ccl2
Fold change
WT gp130Act/IEC
i
Muc2
Area [%]
WT gp130Act/IEC
j
WT
gp130Act/IEC
Muc2
DAPI
Control
Ethanol
k
GAPs
GAPs/Villus [n°]
WT gp130Act/IEC
m
Chrm4
Fold change
WT gp130Act/IEC
n
mAChR4
Fold change (Relative to β-actin)
WT gp130Act/IEC
l
WT
gp130Act/IEC
Muc2
Dextran
DAPI
Control
Ethanol
o
Isolated goblet cells
Ethanol
WT
gp130Act/IEC
mAChR4
β-actin
p
Total bacteria
[16S*µg DNA/mg feces]
WT gp130Act/IEC
q
PCoA_wunifrac
p=0.001
Axis1 [21%]
Axis1 [25%]
WT Control
WT Ethanol
gp130Act/IEC Control
gp130Act/IEC Ethanol

Figure 2. Expression of activated gp130 in IECs prevents ethanol-induced liver disease and promotes GAP formation. (a) *Chrm4* mRNA in small intestinal organoids from WT mice (n= 2) was quantitated by qPCR after stimulation with IL-6 (0.02 μg/ml) in the presence of ethanol (10 mM) for 12 h. 6 technical replicates were pooled in each of two independent biological experiments. (b) mAChR4 protein amounts in WT small intestinal organoids after stimulation without (n=3) or with IL-6 (0.5 μg/ml) (n=3) for 24 h. (c) Representative mAChR4 immunoblots. (d–q) WT mice and $gp130^{Act/IEC}$ littermates were fed control (n=4–15) or ethanol containing Lieber DeCarli diets (n=4–44) for 10 weeks. (d) Plasma levels of ALT. (e) Hepatic triglyceride content. (f) Representative H&E-stained liver sections. *Scale bar* = 200 μm. (g–h) Hepatic *Cxcl1 and Ccl2* mRNAs were quantitated by qPCR. (i) Percentage of Muc2 positive stained area. (j) Representative sections stained with Muc2 antibody (red) showing GCs and DAPI (blue). Scale bar = 200 μm. (k) Number of GAPs per villus. (l) Representative TMR-dextran (red) showing GAPs, Muc2 antibody (green) and DAPI (blue) stained small intestine sections showing GAPs (Arrowheads). *Scale bar* = 25 μm. (m) Small intestinal *Chrm4* mRNA was quantified by qPCR. (n) mAChR4 protein amounts relative to β-actin in isolated GCs. (o) Immunoblots of mAChR4 and β-actin in isolated GCs. (p) Total fecal bacteria were quantitated by qPCR. (q) Principal coordinate analysis (PCoA) with weighted UniFrac of 16S rRNA sequencing of fecal samples. *P* values were determined by One-way ANOVA with Tukey's post-hoc test (d, e, i, k and p), by two-sided unpaired Student *t* test or Mann-Whitney U-statistic test (a, b, g, h, m and n) and by two-sided paired *t* test. Results are expressed as mean ± s.e.m. **P*<0.05.

Figure 3

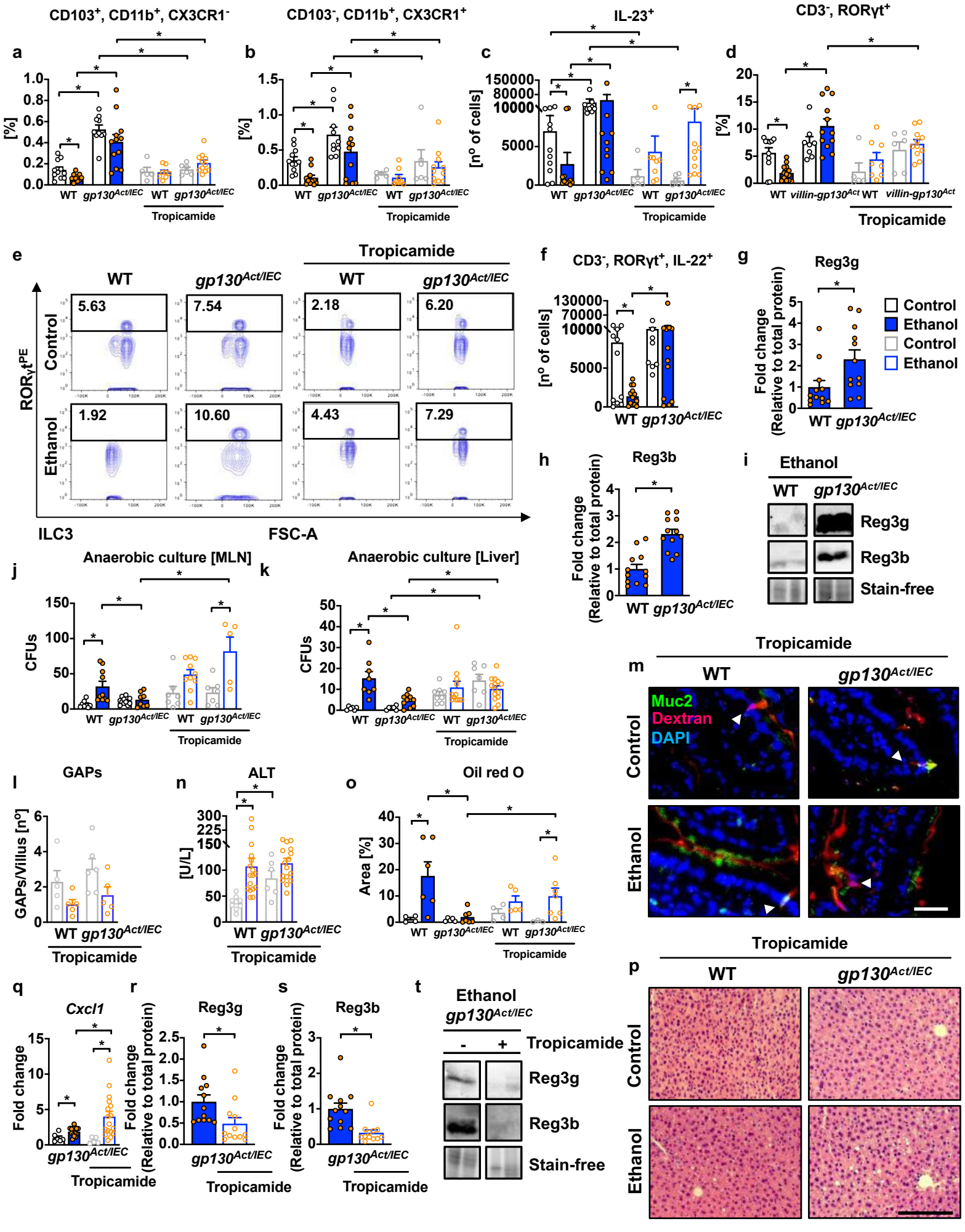
a
CD103+, CD11b+, CX3CR1-
[%]
WT gp130Act/IEC WT gp130Act/IEC
Tropicamide
b
CD103-, CD11b+, CX3CR1+
[%]
WT gp130Act/IEC WT gp130Act/IEC
Tropicamide
c
IL-23+
[nº of cells]
150000
80000
10000
5000
0
WT gp130Act/IEC WT gp130Act/IEC
Tropicamide
d
CD3-, RORγt+
[%]
WT villin-gp130Act WT villin-gp130Act
Tropicamide
e
Tropicamide
WT
gp130Act/IEC
WT
gp130Act/IEC
Control
Ethanol
5.63
7.54
2.18
6.20
1.92
10.60
4.43
7.29
RORγtPE
ILC3
FSC-A
f
CD3-, RORγt+, IL-22+
[nº of cells]
130000
70000
10000
5000
0
WT gp130Act/IEC
g
Reg3g
Fold change (Relative to total protein)
WT gp130Act/IEC
Control
Ethanol
Control
Ethanol
h
Reg3b
Fold change (Relative to total protein)
WT gp130Act/IEC
i
Ethanol
WT gp130Act/IEC
Reg3g
Reg3b
Stain-free
j
Anaerobic culture [MLN]
CFUs
WT gp130Act/IEC WT gp130Act/IEC
Tropicamide
k
Anaerobic culture [Liver]
CFUs
WT gp130Act/IEC WT gp130Act/IEC
Tropicamide
l
GAPs
GAPs/Villus [nº]
WT gp130Act/IEC
Tropicamide
n
ALT
[U/L]
WT gp130Act/IEC
Tropicamide
o
Oil red O
Area [%]
WT gp130Act/IEC WT gp130Act/IEC
Tropicamide
m
Tropicamide
WT
gp130Act/IEC
Control
Ethanol
Muc2
Dextran
DAPI
q
Cxcl1
Fold change
gp130Act/IEC
Tropicamide
r
Reg3g
Fold change (Relative to total protein)
gp130Act/IEC
Tropicamide
s
Reg3b
Fold change (Relative to total protein)
gp130Act/IEC
Tropicamide
t
Ethanol
gp130Act/IEC
- +
Tropicamide
Reg3g
Reg3b
Stain-free
p
Tropicamide
WT
gp130Act/IEC
Control
Ethanol

Figure 3. Expression of activated gp130 in IECs stimulates protective intestinal adaptive immune response via mAChR4-mediated GAP formation. (a–t) WT mice and *gp130*$^{Act/IEC}$ littermates were fed control (n=4–11) or ethanol containing Lieber DeCarli diets (n=6–17) for 10 weeks. (a–d, j–t) A group of littermate mice were treated with the mAChR antagonist tropicamide (20 mg/kg) during the last 29 days (n=5–17). (a–c) Isolated LP immune cells for APC subset identification studies were stimulated with flagellin (100 ng/ml) for 2.5 h. (a–b) Frequencies of tolerogenic APC subsets in total mononuclear phagocyte population were gated according to CD45, MHCII, CD11c, CD103, CD11b, and CX3CR1 expression. (c) Total number of IL-23$^+$ cells in all APCs subsets. (d) Frequencies of ILC3s (CD45$^+$, CD3$^-$, ROR$_\gamma$t$^+$) cells after stimulation of isolated LP leukocytes with mouse IL-23 (40 ng/µl) for 4 h. (e) Representative ILC3 and (f) IL-22 expressing ILC3 plots. (g–h) Quantification of Reg3g and Reg3b protein amounts relative to total protein identified by stain-free imaging technology. (i) Representative Reg3g and Reg3b immunoblots. (j, k) Number of colony forming units (CFU) of anaerobically cultured bacteria from sterile collected mesenteric lymph nodes and liver. (l) Number of GAPs per villus. (m) Representative TMR-dextran (red), Muc2 antibody (green) and DAPI (blue) stained small intestinal sections showing GAPs (Arrowheads). *Scale bar* = 25 µm. (n) Plasma ALT concentrations. (o) Quantification of the Oil red O (ORO)-stained liver sections. (p) Representative H&E stained liver sections. *Scale bar* = 200 µm. (q) Hepatic *Cxcl1* mRNA quantitated by qPCR. (r, s) Reg3g and Reg3b proteins relative to total protein identified by stain-free imaging technology. (t) Representative Reg3g and Reg3b immunoblots. *P* values were determined by two-way (a–d, j–k and o) or one-way ANOVA (f, l, n and q) with Tukey's post-hoc test and by two-sided unpaired Student *t* test or Mann-Whitney U-statistic test (g, h, r and s). Results are expressed as mean ± s.e.m. **P*<0.05.

Figure 4

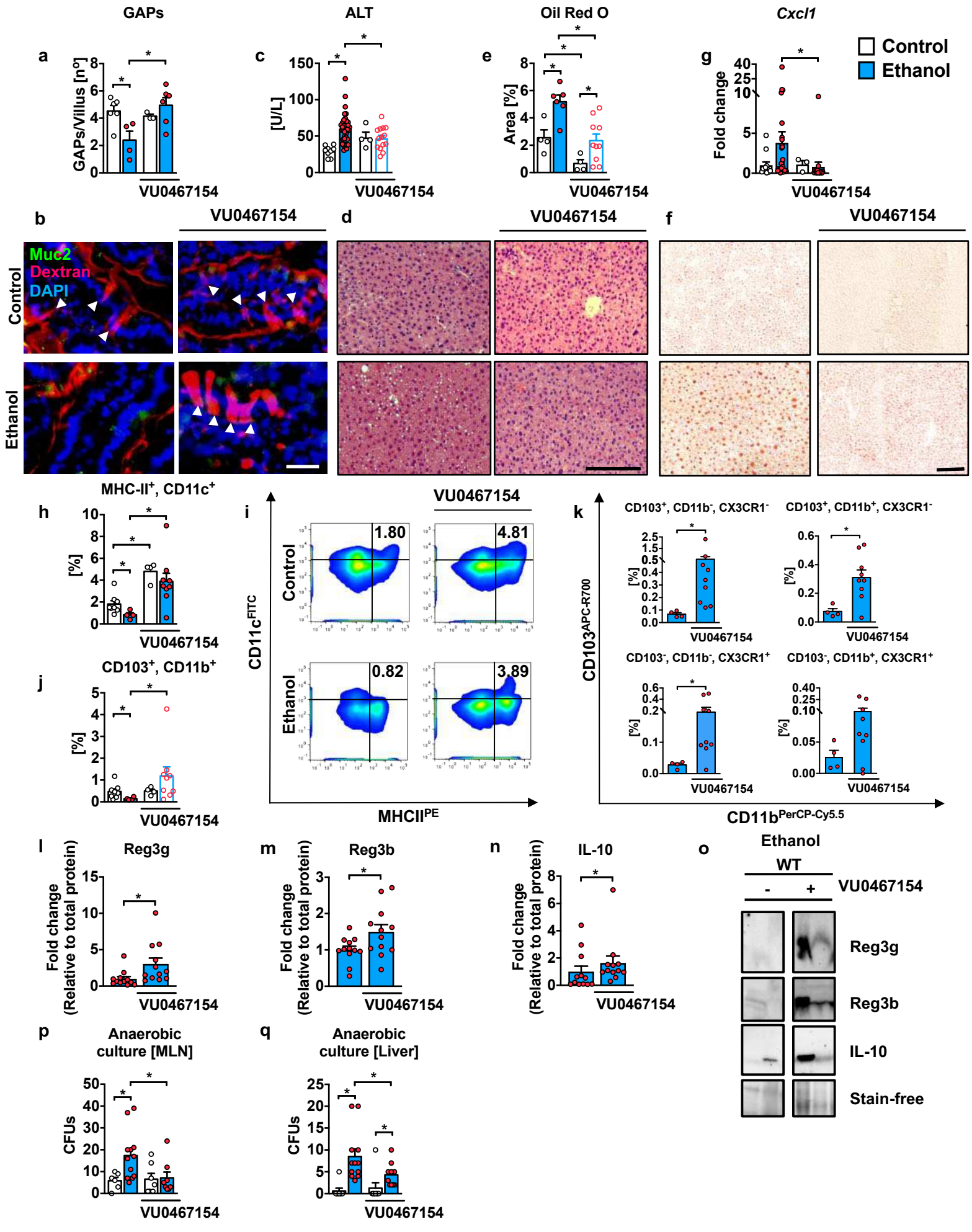
GAPs
ALT
Oil Red O
Cxcl1
Control
Ethanol
a
GAPs/Villus [n°]
VU0467154
c
[U/L]
e
Area [%]
g
Fold change
b
VU0467154
Muc2
Dextran
DAPI
Control
Ethanol
d
f
MHC-II+, CD11c+
h
[%]
i
1.80
4.81
0.82
3.89
CD11cFITC
MHCIIPE
k
CD103+, CD11b-, CX3CR1-
CD103+, CD11b+, CX3CR1-
CD103-, CD11b-, CX3CR1+
CD103-, CD11b+, CX3CR1+
CD103APC-R700
CD11bPerCP-Cy5.5
j
CD103+, CD11b+
l
Reg3g
Fold change (Relative to total protein)
m
Reg3b
n
IL-10
o
Ethanol
WT
-
+
Reg3g
Reg3b
IL-10
Stain-free
p
Anaerobic culture [MLN]
CFUs
q
Anaerobic culture [Liver]

Figure 4. A mAChR4 PAM reduces ethanol-induced liver disease. WT mice were fed control (n=3–9) or ethanol containing Lieber DeCarli diets (n=4–38) for 10 weeks in the presence or absence of the specific mAChR4 PAM VU0467154 (5 mg/Kg), dissolved in the diet during the last 29 days. (a) Number of GAPs per villus. (b) Representative TMR-dextran (red), Muc2 (green) and DAPI (blue) stained small intestine sections showing GAPs (Arrowheads). *Scale bar* = 25 μm. (c) Plasma ALT concentrations. (d) Representative H&E stained liver sections. *Scale bar* = 200 μm. (e) Quantification of ORO-stained liver sections. (f) Representative oil ORO-stained liver sections. *Scale bar* = 100 μm. (g) Hepatic *Cxcl1* mRNA amounts. (h–k) DCs were stimulated with flagellin (100 ng/ml) for 2.5 h before staining. (h) Frequencies of $CD45^+$, $MHCII^+$, $CD11c^+$ APCs in total mononuclear phagocyte population. (i) Representative APCs plots. (j) Frequencies of $CD45^+$, $MHCII^+$, $CD11c^+$, $CD103^+$, $CD11b^+$ DCs. (k) Frequencies of tolerogenic APC subsets according to CD45, MHCII, CD11c, CD103, CD11b and CX3CR1 expression. (l–n) Quantification of Reg3g, Reg3b and IL-10 proteins relative to total protein identified by stain-free imaging technology. (o) Representative Reg3g, Reg3b, and IL-10 immunoblots. (p, q) Number of CFUs of anaerobically cultured bacteria from sterile collected MLNs and liver. *P* values were determined by one-way ANOVA (a, c, e, g, h, j, p, q) with Tukey's post-hoc test and by two-sided unpaired Student *t* test or Mann-Whitney U-statistic test (k, l-n). Results are expressed as mean ± s.e.m. $*P<0.05$.

Methods

Human study. Duodenal biopsies from fifteen patients with AUD and eight biopsies from non-alcoholic controls were obtained from the alcohol withdrawal unit of Cliniques Universitaires Saint-Luc, Brussels, Belgium where they followed a highly standardized detoxification and rehabilitation program. The demographic data for controls and patients as well as clinical and laboratory characteristics for patients are shown in Extended Data Table 1. AUD patients showed a wide range of liver involvement ranging from minimal liver disease to steatohepatitis or steatofibrosis but no patient had cirrhosis (Extended Data Table 2). Patients were actively drinking until the day of admission. Exclusion criteria included antibiotics use during the two months preceding enrollment, immunosuppressive medication, diabetes, inflammatory bowel disease, known liver disease of any other etiology, and clinically significant cardio-vascular, pulmonary or renal co-morbidities. Written informed consent was obtained from all patients and controls. The study protocol was approved by the Ethics Committee of the Université Catholique de Louvain, in Brussels, Belgium. Duodenal biopsies were obtained during an upper gastro-intestinal endoscopy performed at day 2 of admission. Samples were fixed in 10% formalin and were paraffin-embedded. To visualize GCs in humans, we used Periodic Acid/Schiff (PAS) staining. Slides were digitalized using a SCN400 slide scanner (Leica Biosystems, Wetzlar, Germany) at x20 magnification and subjected to analysis with the image analysis tool Author version 2017.2 (Visiopharm, Hørsolm, Denmark).

Mice. C57BL/6 mice were purchased from Charles River and used in Figure 1. WT C57BL/6 mice bred at the UCSD animal facility were used in Figure 4 and Extended Data Figure 5. All mice used in other figures were bred in the same animal facility. *gp130*$^{Act/IEC}$ mice on a C57BL/6 background

459 have been described before [7]. *gp130*$^{Act/IEC}$ males and WT littermate females were used for breeding.
460 Littermates were used throughout this study except for ILC3 analysis where 6 non-littermate
461 C57BL/6 WT were included in each group.
462 Female mice (age, 8 weeks) were placed on Lieber DeCarli diet for 10 weeks as previously
463 described [8]. In brief, the Lieber DeCarli diet comprises Micro Stabilized Rod Liq AC IRR
464 (LD101A; TestDiet), Maltodextrin IRR (9598; TestDiet) and 200-proof ethanol (Koptec). The
465 caloric intake from ethanol was 0 on day 1, 10% of total calories on days 2 and 3, 20% on days 4
466 and 5, 30% from day 6 until the end of 6 weeks, and 36% until the end of the treatment. Control
467 mice received an isocaloric amount of iso-maltose instead of ethanol.
468 To study the effect of tropicamide, *gp130*$^{Act/IEC}$ mice and corresponding WT littermate mice fed
469 Lieber DeCarli diet containing ethanol or isocaloric iso-maltose for 10 weeks were treated with
470 the mAChR4 antagonist tropicamide (20 mg/kg), which was dissolved in the diet for the last 29
471 days.
472 To enhance GAP formation, WT C57BL/6 mice fed Lieber DeCarli diet containing ethanol or
473 isocaloric iso-maltose for 10 weeks were treated for the last 29 days with the specific mAChR4
474 PAM VU0467154 (5 mg/kg), which was dissolved in the liquid diet.
475 Mice were pair-fed and the amount of liquid diet containing ethanol was similar between mouse
476 strains within each experiment (Extended Data Fig. 1a and Extended Data Fig. 5a). Activation of
477 gp130 in IEC did not affect ethanol absorption (Extended Data Fig. 1b). The use of tropicamide
478 or VU0467154 did not affect ethanol absorption (Extended Data Fig. 1b and Extended Data Fig.
479 5b)
480 All animal studies were reviewed and approved by the UCSD Institutional Animal Care and Use
481 Committee.

Bacterial DNA isolation and 16S rRNA sequencing. DNA was isolated from feces of mice. Samples were resuspended in phosphate-buffered saline (PBS) and digested with RNAse A and proteinase K at 55°C for one hour. Each suspension was then transferred to individual Qbiogene lysing matrix B tubes and vortexed using a FastPrep FP120 instrument. The lysate was then extracted twice using Phenol/Chloroform/Isoamyl alcohol, precipitated and washed with ethanol, and the DNA resuspended in TE buffer [34-36]. 16S ribosomal RNA (rRNA) PCR was completed using Illumina adaptor and barcode ligated 16S primers targeting the V4 region of the 16S rRNA gene [9,34,37,38]. Amplicons were purified using the Qiaquick PCR purification kit (QIAGEN) following manufacturer's specifications. Purified amplicons were then quantified via TECAN assay (Tecan, Switzerland), normalized, and pooled in preparation for 16S rRNA sequencing. The pooled library was quantified and checked for quality using Agilent 2100 Bioanalyzer (Agilent Technologies) and sequenced on Illumina MiSeq (Illumina) using V2 reagent chemistry, 500 cycles, 2 x 250bp format using manufacturer's specifications. 16S sequence reads were processed and OTUs were determined using our MOTHUR-based 16S rDNA analysis workflow as described [8,34,36]. Raw 16S sequence reads can be found in the NCBI SRA associated with Bioproject PRJNA705611 and BioSample IDs: SAMN18094194-SAMN18094231.

Determination of bacterial translocation. Translocation of viable bacteria was assessed by culturing MLNs and liver[34]. Sterile MLNs and liver were homogenized using a bead beater (1.0 mm zirconia/silica beads) under sterile and anaerobic conditions and kept for 1.5 h at 37°C in a bacterial incubator. Different dilutions were plated on CDC Anaerobe 5% Sheep Blood Agar with

Phenylethyl Alcohol (PEA) plates inside of an anaerobic workstation and cultured anaerobically at 37°C for 72 h.

Staining procedures. Formalin-fixed tissue samples were embedded in paraffin (Paraplast plus, McCornick) and stained with H&E (Surgipath). To determine lipid accumulation, liver sections were embedded in OCT (Tissue-Tek^{R}) compound. 5 μm frozen sections were then cut and stained with Oil Red O (Sigma-Aldrich). Representative pictures from each group of mice are shown in each figure. All samples were analyzed by densitometry, using National Institutes of Health (NIH) Image J.

For immunofluorescence staining, tissues were fixed in 10% buffered formalin, embedded in paraffin and sectioned at 5 μm thickness and stained with anti-Muc2 (1:200) (San Cruz Biotechnology) primary antibody, or anti-mAChR4 (1:200) (Alomone labs) overnight, or anti-GFP antibody (1:200) (Abcam) and then, incubated with Alexa fluor 568- or Alexa fluor 488-conjugated secondary antibodies (Invitrogen). Nuclei were stained in blue with a Vectashield^{R} (Vector Laboratories) mounting medium containing DAPI and imaged by fluorescent microscopy. Control sections were stained with isotype antibody and showed no staining. All samples were analyzed by densitometry, using NIH Image J.

To enumerate GAPs a 2 cm small intestinal loop was clipped and injected with 200 μl of 10 mg/ml tetramethylrhodamine (TMR)-dextran 10,000 MW, lysine fixable (Thermo Scientific). Next, tissue was fixed in 10% formalin overnight and subsequently embedded in OCT for frozen sectioning (5 μm) for Muc2 immunofluorescence staining as above. Number of GAPs were identified as TMR-dextran-filled columns measuring approximately 20 μm (height) x 5 μm (diameter) traversing the epithelium and containing a nucleus. Small intestinal GAPs were

enumerated as GAPs per villus. To evaluate the intercommunication of bacteria with LP-immune cells via GAPs, 5 x 10^9 *E. faecalis* genetically modified with an EGFP vector were gavaged at 3 and 0.5 h before the end of the study. Trans-epithelial dextran columns did not cause disruption of the epithelial barrier as shown by the exclusion of dextran from the LP.

Bacterial culture. *E. faecalis* was genetically modified with an EGFP reporter plasmid pBSU101 [39]. EGFP-*E. faecalis* were grown in brain heart infusion (BHI) broth or on BHI agar plate at 37°C with 125 μg/ml spectinomycin (Sigma). 5 x 10^9 CFUs were gavaged as indicated in figure legends.

Real-time quantitative PCR. RNA was extracted from mouse tissues and cDNA was generated [9]. Primer sequences for mouse genes were obtained from the NIH qPrimerDepot. All primers used in this study are listed in Extended Data Table 3. Gene expression was determined with Sybr Green (Bio-Rad Laboratories) using ABI StepOnePlus real-time PCR system. The qPCR value was normalized to *Tbp* or 18S housekeeping genes. To quantify the total bacterial load in feces, the qPCR value of 16S rRNA gene for each sample was multiplied by the total amount of DNA (μg) mg^{-1} of feces. Published bacterial primer sequences were used for 16S rRNA gene [40] (Extended Data Table 3).

Biochemical analysis. Plasma levels of ALT were determined with Infinity ALT kit (Thermo Scientific). Hepatic triglyceride levels were measured using Triglyceride Liquid Reagents kit (Pointe Scientific). Plasma levels of ethanol were measured using Ethanol Assay kit (BioVision).

549 **Goblet cell isolation.** GCs were isolated by selection of biotinylated cytokeratin 18 (CK18)
550 (Abcam) [41], which is highly expressed in GCs, with streptavidin magnetic beads after isolation of
551 small intestinal cells using a solution containing HBSS without Ca^{2+} and Mg^{2+}, 1M HEPES, 100
552 mM sodium pyruvate and 0.5 M EDTA. Magnitude of GC enrichment was confirmed (Extended
553 Data Fig. 1c–1d).
554
555 **Small intestinal organoid isolation and culture.** Small intestinal crypts were isolated from WT
556 mice, cultured and stained as described [42] and treated with ethanol (10 mM) and/or IL-6 (0.02, 0.1
557 and 0.5 μg/ml) (Biolegend) for 12h or 24h.
558
559 **Flow cytometry.** Isolation: Small intestine was harvested, and the epithelial cell layer was
560 removed. Pieces were digested in media containing 1 mg/mL collagenase (Millipore Sigma), 0.1
561 U/mL dispase (Worthington Biochem) and 0.1 mg/mL DNase I (Millipore Sigma) at 37°C at 150
562 rpm for 30 min. A 40% and 80% Percoll gradient was used to collect the lymphoid fractions at the
563 interphase. Flow cytometry: LP-immune cells were pelleted and blocked with anti-mouse
564 CD16/32 antibody (Thermo Fisher) for 15 min. Cells were divided to perform 3 different panels
565 to analyze APCs, ILC3s and Tregs. Stimulation and staining: To stimulate IL-23 secretion by LP-
566 APCs, cells were re-stimulated *in vitro* with 100 ng/ml flagellin (Invivogen) for 2.5 h in the
567 presence of 0.7 μl/ml BD GolgiStop™ (BD Bioscience) to accumulate cytokines and/or proteins.
568 The murine APC panel consisted of CD45.2 (V500, clone 104, BD), CD11c (FITC, clone N418,
569 ThermoFisher), MHC Class II (I-A/I-E) (PE, clone M5/114.15.2, ThermoFisher), CD11b (PerCP-
570 Cy5.5, clone M1/70, BD), CD103 (APC-R700, clone M290, BD), CX3CR1 (BV421, clone

SA011F11, BioLegend), fixable viability stain (FVS) (575V, BD), IL-10 (BV711, clone JES5-16E3, BD) and IL-23 p19 (AF647, clone N71-1183).

In parallel, another set of isolated LP-immune cells was stimulated with 40 ng/µl of recombinant mouse IL-23 (Biolegend) for 4 h in the presence of 0.7 µl/ml BD GolgiStop™ (BD Bioscience) to stimulate IL-22 secretion. ILC3 panel consisted of CD45.2 (V500, clone 104, BD), CD3e (FITC, clone 17A2, PharMingen), FVS (575V, BD), IL-22 (APC, clone IL22JOP, ThermoFisher) and RORγt (PE, clone B2D, ThermoFisher).

Another set of isolated LP-immune cells were stimulated with 10 ng/ml phorbol 12-myristate 13-acetate (PMA) (Sigma-Aldrich) plus 500 ng/ml ionomycin (Sigma-Aldrich) for 4 h in the presence of 0.7 µl/ml BD GolgiStop™ (BD Bioscience). The third panel consisted of FVS (575V, BD), CD45.2 (V500, clone 104, BD), CD4 (BUV496, clone GK1.5, BD), CD25 (APC-R700, clone PC61, BD), FOXP3 (BV421, clone MF-14, BioLegend).

Cells were stained with the corresponding antibodies against the surface receptors of interest for 30 min following permeabilization and intracellular staining of cytokines or receptors for 30 min. Cells were recorded using FACS Celesta and LSR Fortessa (BD) flow cytometers at the Flow Cytometry Core Facility at the La Jolla Institute for Immunology (La Jolla, CA). Data was analyzed using FlowJo (version 10.5.3).

Immunoblot analyses. To measure expression levels of mAChR4, GCs were isolated as described above. Immunoblot analysis was performed as described [34] using anti-AChR4 1:1000 (#AMR-004; Alomone labs) and anti-β-actin 1:5000 (Sigma-Aldrich) antibody as loading control. Protein from proximal small intestine was extracted and immunoblot analysis was performed using anti-Reg3g 1:500 (ab198216, Abcam), anti-Reg3b 1:500 (ABIN1870289, Antibodies online), and anti-

IL-10 1:1000 (sc-365858; Santa Cruz Biotechnology) antibodies. Stain-free imaging technology using polyacrylamide gels (BioRad) containing a proprietary trihalo compound to make proteins fluorescent, was employed to calculate total protein. Immunoblots were visualized with a charged coupling device camera in a luminescent image analyzer (Gel-Doc; Bio-Rad). Immunoblots were analyzed by densitometry, using Image Lab version 6.0.1 software (Bio-Rad).

Data availability. Raw 16S sequence reads can be found in the NCBI SRA associated with Bioproject PRJNA705611 and BioSample IDs: SAMN18094194-SAMN18094231.

Statistical analysis. Results are expressed as mean ± s.e.m. Significance of two groups or multiple groups were evaluated using two-sided unpaired Student's t-test, two-sided unpaired Mann-Whitney test, or one-way or two-way analysis of variance (ANOVA) with Tukey's post-hoc test, respectively. Statistical analyses were performed using R statistical software, R v.3.5.1 (R Foundation for Statistical Computing) and GraphPad Prism v9.01. A $P<0.05$ was considered to be statistically significant (adjusted for multiple comparison when performing multiple tests).

Method references

34 Yan, A. W. *et al.* Enteric dysbiosis associated with a mouse model of alcoholic liver disease. *Hepatology* **53**, 96-105, doi:10.1002/hep.24018 (2011).

35 Fouts, D. E., Torralba, M., Nelson, K. E., Brenner, D. A. & Schnabl, B. Bacterial translocation and changes in the intestinal microbiome in mouse models of liver disease. *J Hepatol* **56**, 1283-1292 (2012).

36 Chen, P. *et al.* Supplementation of saturated long-chain fatty acids maintains intestinal eubiosis and reduces ethanol-induced liver injury in mice. *Gastroenterology* **148**, 203-214 (2015).

37 Haas, B. J. *et al.* Chimeric 16S rRNA sequence formation and detection in Sanger and 454-pyrosequenced PCR amplicons. *Genome Res* **21**, 494-504, doi:10.1101/gr.112730.110 gr.112730.110 [pii] (2011).

38 Caporaso, J. G. *et al.* Global patterns of 16S rRNA diversity at a depth of millions of sequences per sample. *Proceedings of the National Academy of Sciences of the United States of America* **108 Suppl 1**, 4516-4522, doi:10.1073/pnas.1000080107 1000080107 [pii] (2011).

39 Aymanns, S., Mauerer, S., van Zandbergen, G., Wolz, C. & Spellerberg, B. High-level fluorescence labeling of gram-positive pathogens. *PLoS One* **6**, e19822, doi:10.1371/journal.pone.0019822 (2011).

40 Maeda, H. *et al.* Quantitative real-time PCR using TaqMan and SYBR Green for Actinobacillus actinomycetemcomitans, Porphyromonas gingivalis, Prevotella intermedia, tetQ gene and total bacteria. *FEMS Immunol Med Microbiol* **39**, 81-86, doi:S0928824403002244 [pii] (2003).

41 Knoop, K. A. *et al.* Microbial antigen encounter during a preweaning interval is critical for tolerance to gut bacteria. *Sci Immunol* **2**, doi:10.1126/sciimmunol.aao1314 (2017).

42 Sato, T. *et al.* Single Lgr5 stem cells build crypt-villus structures in vitro without a mesenchymal niche. *Nature* **459**, 262-265, doi:10.1038/nature07935 (2009).

Acknowledgments

This study was supported by the American Association for the Study of Liver Diseases (AASLD) Pinnacle Research Award in Liver Disease (8998GA), by the Southern California Research Center for Alcoholic Liver and Pancreatic Diseases (ALPD) and Cirrhosis (P50 AA011999) funded by the National Institute on Alcohol Abuse and Alcoholism (NIAAA) and its Animal Core facilities, and the Isenberg Endowed Fellowship jointly awarded by the Pilot/Feasibility Program of the San Diego Digestive Diseases Research Center (SDDRC) and the Hellman Family Foundation (P30 DK120515) (to C.L.). This study was supported in part by JSPS KAKENHI (JP 15K21775, JP 20H03758), AMED (PRIME) under Grant Number JP

18gm6210008/19gm6210008/20gm6210008/21gm6210008 (to K.T.). This study was supported in part by grants from Fond National de Recherche Scientifique Belgium (J.0146.17 and T.0217.18) and Action de Recherche Concertée (ARC), Université Catholique de Louvain, Belgium (to P.S). This study was supported in part by NIH grants U01 027681, R01 CA234128, R37 AI043477 (to M.K.), R01 AA24726, R01 AA020703, U01 AA026939, by Award Number BX004594 from the Biomedical Laboratory Research & Development Service of the VA Office of Research and Development, and a Biocodex Microbiota Foundation Grant (to B.S.).

Author Contributions

C. L. was responsible for acquisition, analysis and interpretation of data, study concept and design and drafting of the manuscript; R. B., N. C., R. B-C., N. P., L. M., A. A., R. Z. and Y. D provided assistance on data acquisition; B. G. was responsible for 16S rRNA sequencing data analysis, K. T. created the *gp130*$^{Act/IEC}$ mouse model, R. N, D. A. B., and M. K. provided scientific advice and technical support, D. E. F. was responsible for 16S rRNA sequencing, P.S. was responsible for collection of human samples, B.S. and M.K. were responsible for the study concept and design, study supervision and editing the manuscript.

Declaration of Interests

B.S. has been consulting for Ferring Research Institute, HOST Therabiomics, Intercept Pharmaceuticals, Mabwell Therapeutics, Patara Pharmaceuticals and Takeda. B.S.'s institution UC San Diego has received grant support from Axial Biotherapeutics, BiomX, CymaBay Therapeutics, NGM Biopharmaceuticals, Prodigy Biotech and Synlogic Operating Company. B.S. is founder of Nterica Bio.

Materials & Correspondence

Michael Karin, Ph.D., Departments of Pharmacology and Pathology, University of California San Diego, MC0723, 9500 Gilman Drive, La Jolla, CA 92093, USA, Phone 858-534-1361, Fax 858-534-8158, Email karinoffice@ucsd.edu

Bernd Schnabl, M.D., Department of Medicine, University of California San Diego, MC0063, 9500 Gilman Drive, La Jolla, CA 92093, Phone 858-822-5311, Fax 858-822-5370, Email beschnabl@ucsd.edu.

Extended Data Figure 1

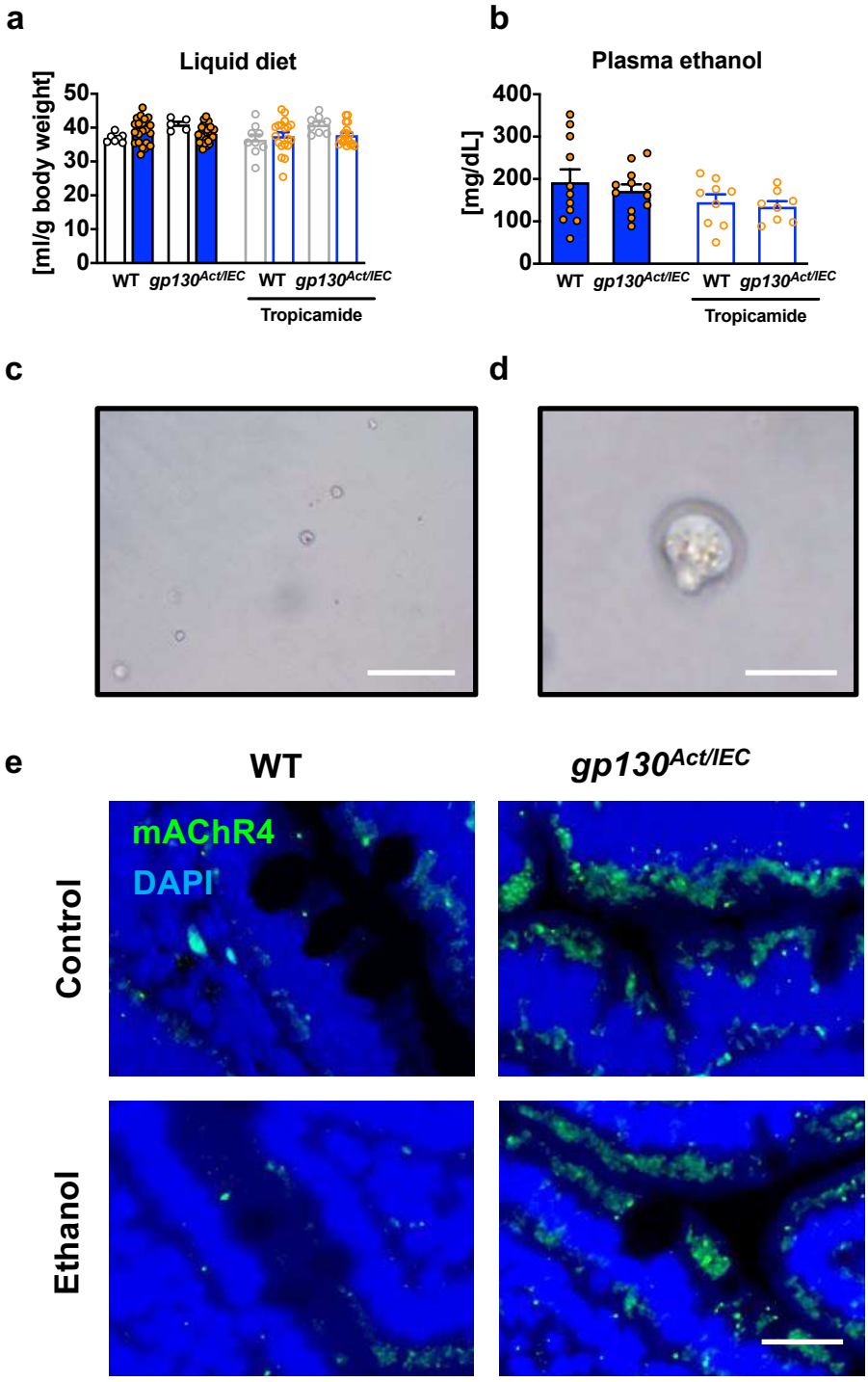

Extended Data Figure 1. Food intake and plasma ethanol level in mice expressing active gp130 in IECs after treatments. (a–e) WT mice and their *gp130*$^{Act/IEC}$ littermates were fed an oral control diet (n=5–7) or ethanol containing Lieber DeCarli diet (n=11–27) for 10 weeks. (a–b) A group of littermate mice were treated with the mAChR4 inhibitor tropicamide (20 mg/kg) during the last 29 days as interventional approach (n=8–19). (a) Food intake of liquid diet. (b) Levels of ethanol in plasma. (c, d) Representative images of isolated goblets cell fraction. (c) *Scale bar* = 100 μm, (d) *Scale bar* = 20 μm. (e) Representative sections of mAChR4 (green) and DAPI (blue) immunofluorescence staining showing distribution of the receptors in GCs. *Scale bar* = 20 μm. *P* values were determined by two-way (a) or one-way ANOVA (b) with Tukey's post-hoc test. Results are expressed as mean ± s.e.m. **P*<0.05.

Extended Data Figure 2

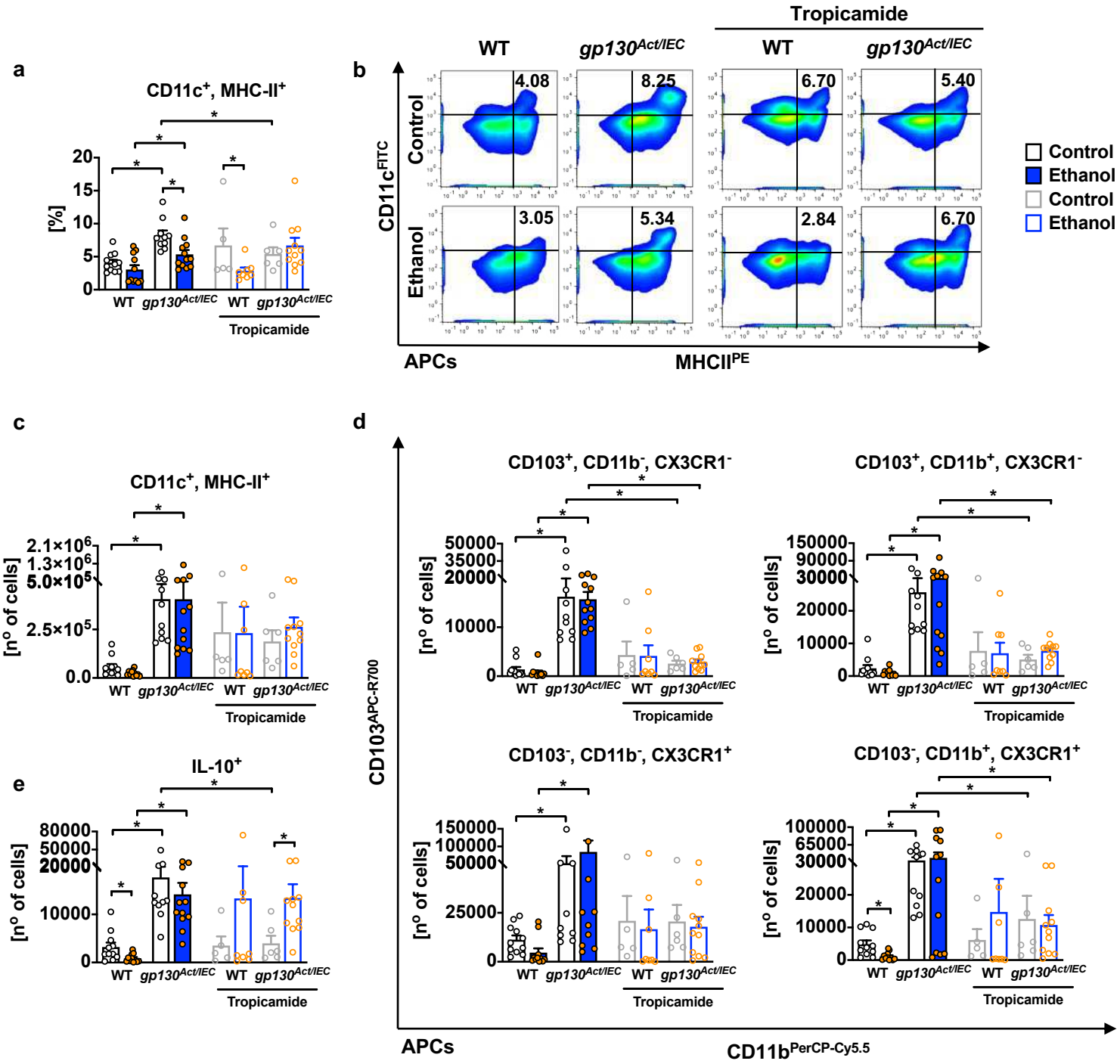

Extended Data Figure 2. Expression of active gp130 in IECs regulates LP-APCs in small intestine. (a–d) WT mice and their *gp130*$^{Act/IEC}$ littermates were fed an oral control diet (n=10–11) or ethanol containing Lieber DeCarli diet (n=11–12) for 10 weeks. A group of littermate mice were treated with mAChR4 inhibitor tropicamide (20 mg/kg) during the last 29 days as interventional approach (n=5–11). LP immune cells were isolated and stimulated with flagellin (100 ng/ml) for 2.5h. (a) Frequencies of APCs (CD45$^+$, MHCII$^+$, CD11c$^+$) at the gate. (b) Representative APCs plots. (c) Total number of APCs (CD45$^+$, MHCII$^+$, CD11c$^+$). (d) Total numbers of subsequently gated APCs (CD45$^+$, MHCII$^+$, CD11c$^+$) according to CD103, CD11b and CX3CR1 expression markers. (e) Total number of IL-10 expressing cells from all the APCs subsets. *P* values were determined by two-way ANOVA with Tukey's post-hoc test. Results are expressed as mean ± s.e.m. *P<0.05.

Extended Data Figure 3

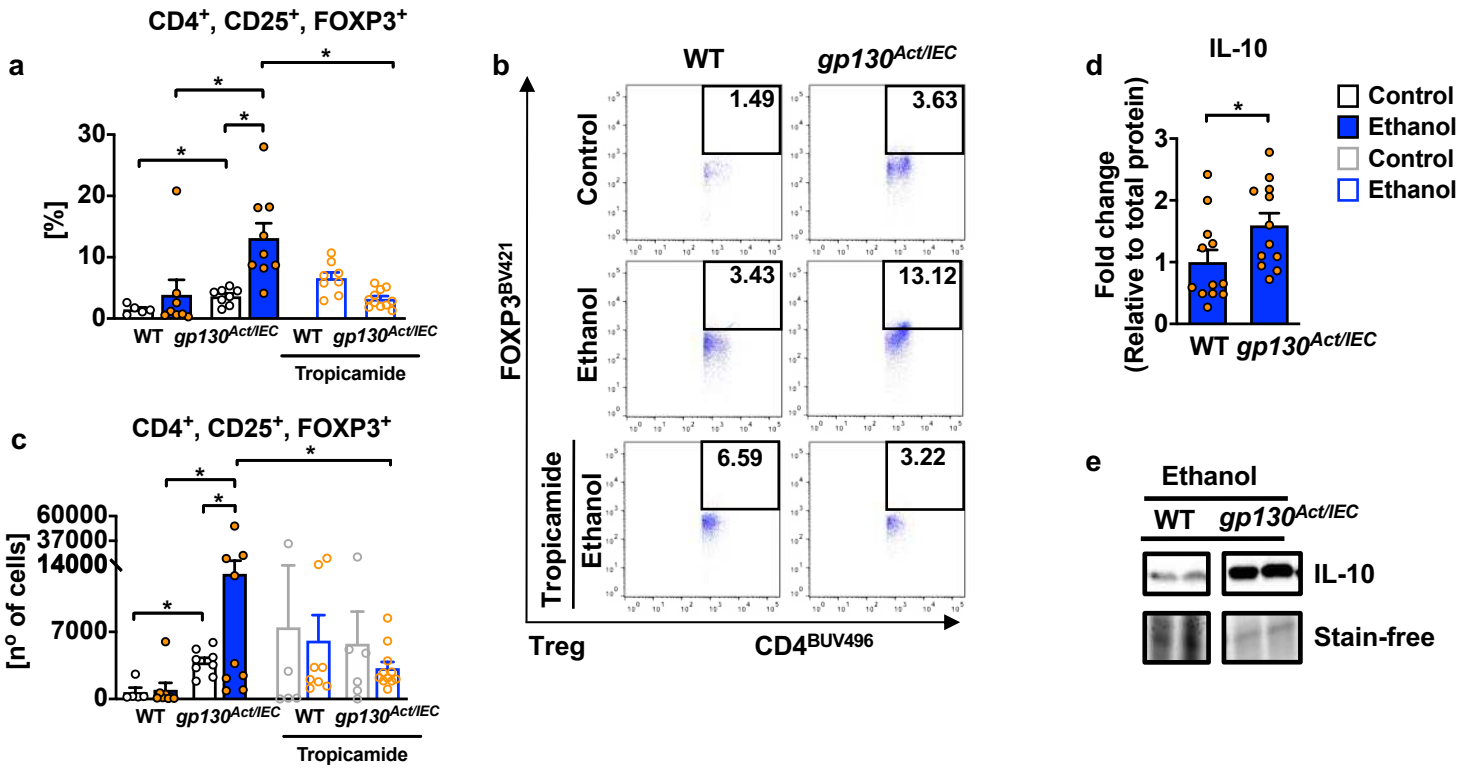

Extended Data Figure 3. Expression of active gp130 in IECs regulates LP- Tregs in small intestine. (a–d) WT mice and their *gp130*$^{Act/IEC}$ littermates were fed an oral control diet (n=5–8) or ethanol containing Lieber DeCarli diet (n=8–12) for 10 weeks. A group of littermate mice were treated with mAChR4 inhibitor tropicamide (20 mg/kg) during the last 29 days as interventional approach (n=5–11). (a-c) Cells were stimulated with PMA (10 ng/ml) plus ionomycin (500 ng/ml) for 4h. (a) Frequencies at the gate of Tregs ($CD4^+$, $CD25^+$ and $FOXP3^+$). (b) Representative Treg plots. (c) Total numbers of Tregs ($CD4^+$, $CD25^+$ and $FOXP3^+$). (d) Quantification of IL-10 protein levels relative to total protein identified with stain-free imaging technology. (e) Representative IL-10 blots. *P* values were determined by two-way ANOVA with Tukey's post-hoc test (a and c) and by two-sided unpaired Student *t* test or Mann-Whitney U-statistic test (d). Results are expressed as mean ± s.e.m. *$P<0.05$.

Extended Data Figure 4

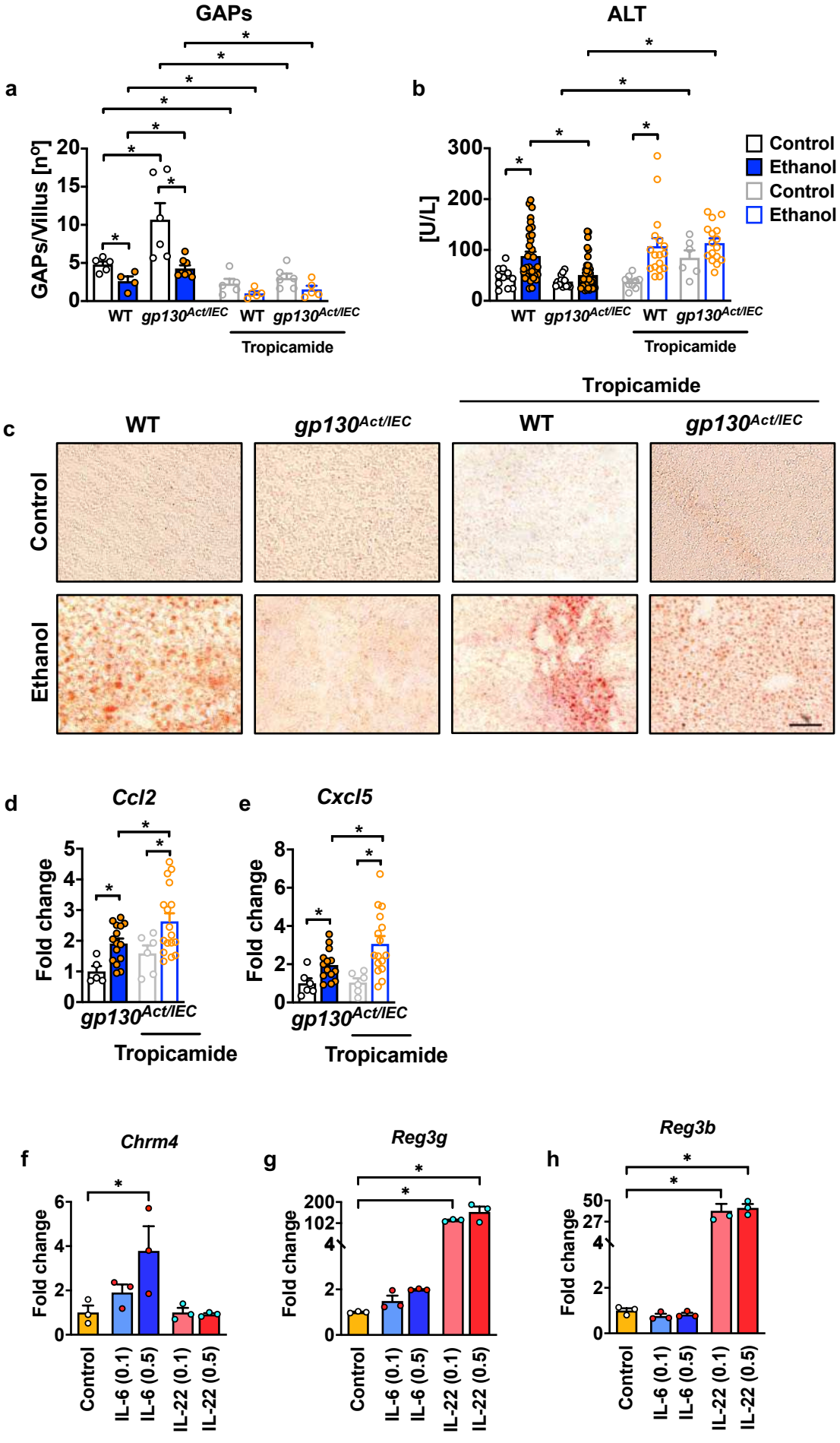

Extended Data Figure 4. Tropicamide-mediated inhibition of small intestinal GAPs reverts the protection against ethanol-induced liver injury in *gp130*$^{Act/IEC}$ mice. (a–e) WT mice and their *gp130*$^{Act/IEC}$ littermates were fed an oral control diet (n=5–15) or ethanol containing Lieber DeCarli diet (n=4–44) for 10 weeks. (a–e) A group of littermate mice were treated with the mAChR4 inhibitor tropicamide (20 mg/kg) during the last 29 days as interventional approach (n=6–17). (a–b) Representation of already described data, now showing all groups in one graph for comparison. (a) Number of GAPs per villus. (b) Plasma levels of ALT. (c) Representative ORO-stained liver sections. *Scale bar* = 100 μm. (d–e) Hepatic *Ccl2* and *Cxcl5* mRNA expression by qPCR. (f–h) *Chrm4*, *Reg3g* and *Reg3b* mRNA in small intestinal organoids from WT mice (n= 3) was quantitated by qPCR after stimulation with IL-6 (0.1 and 0.5 μg/ml) for 24 h. *P* values were determined by two-way (a, b) or one-way ANOVA (d–h) with Tukey's post-hoc test. Results are expressed as mean ± s.e.m. **P*<0.05.

Extended Data Figure 5

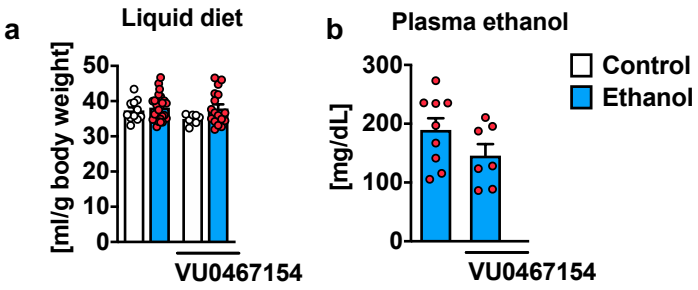

Extended Data Figure 5. Food intake and plasma ethanol level in mice after mAChR4 PAM treatment. (a–b) WT mice were fed an oral control diet (n=7–11) or ethanol containing Lieber DeCarli diet (n=7–27) for 10 weeks in the presence or absence of a specific mAChR4 positive allosteric modulators, VU0467154 (5 mg/Kg), dissolved in the diet during the last 29 days as interventional approach. (a) Food intake of liquid diet. (b) Levels of ethanol in plasma. *P* values were determined by one-way ANOVA (a) with Tukey's post-hoc test and by two-sided unpaired Student *t* test or Mann-Whitney U-statistic test (b). Results are expressed as mean ± s.e.m. **P*<0.05.

Extended Data Figure 6

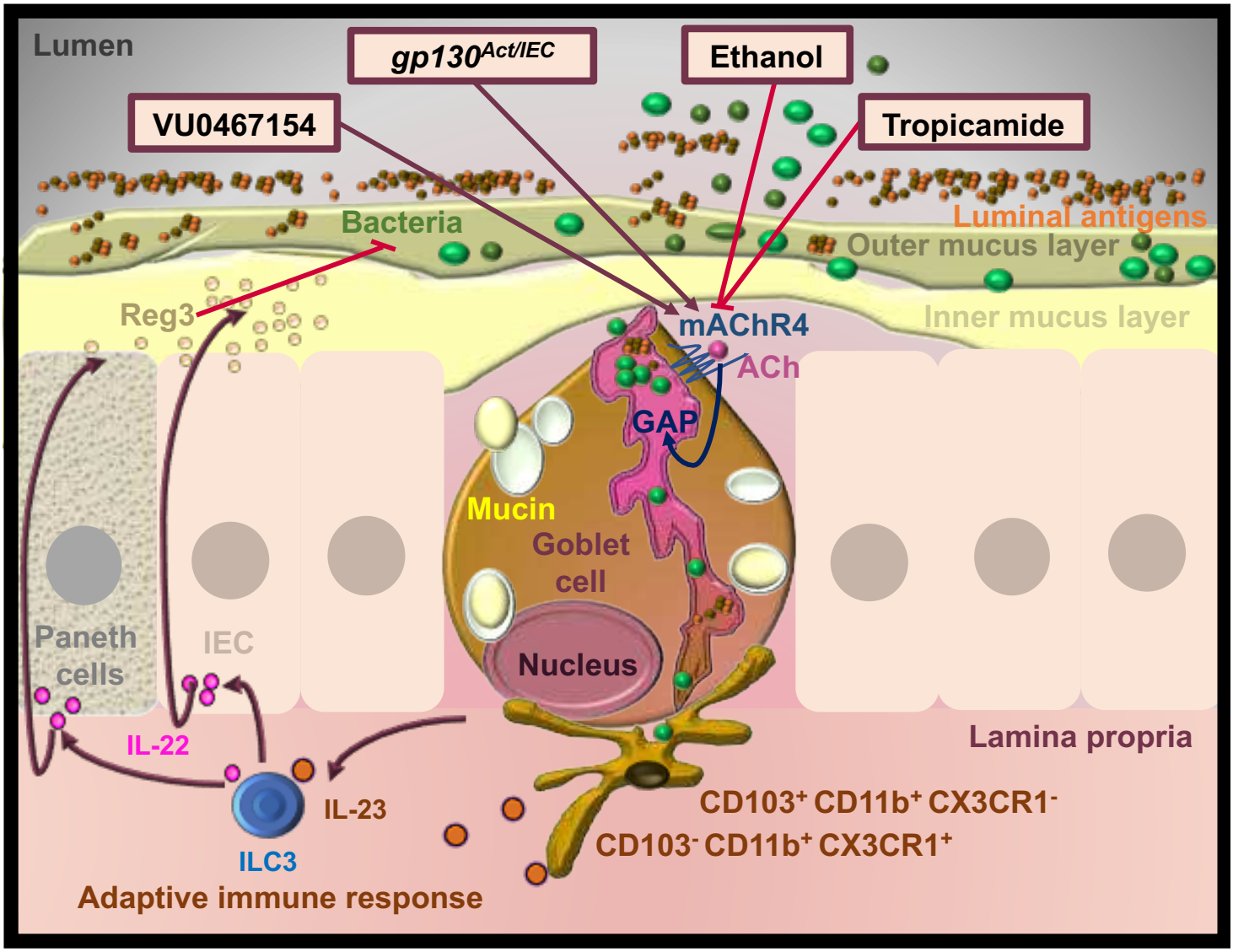

Extended Data Figure 6. Graphical abstract. Upon mucin secretion, goblet cells (GCs) form GC associated antigen passages (GAPs) in response to acetylcholine (ACh) acting on muscarinic ACh receptor 4 (mAChR4). GAPs deliver luminal antigens and bacteria to subjacent tolerogenic $CD103^{+}$, $CD11b^{+}$, $CX3CR1^{-}$ DC subset and $CD103^{-}$, $CD11b^{+}$, $CX3CR^{+}$ APCs. Training of these specific LP-APC subsets by GAPs-mediated delivered antigens induces IL-23 secretion which in turn triggers IL-22 production by type 3 innate lymphoid cells (ILC3s) and stimulation of Reg3 antimicrobial peptides. This particular adaptive immune response promotes an antibacterial defense, prevents ethanol-induced bacterial translocation to the liver and ameliorates ethanol-induced liver disease. Ethanol-induced suppression of mAChR4 and the mAChR4 antagonist tropicamide inhibit GAP formation. Intestinal IL-6 signal transducer (IL6ST/gp130) signaling and the mAChR4 positive allosteric modulator (PAM), VU0467154, stimulate GAP formation, which offers a promising option to prevent the progression of alcohol-related liver disease through regulation of the intestinal immune response.

Extended Data Table 1: Demographic and laboratory results of non-alcoholic controls and patients with alcohol use disorder (AUD).

Variables	Controls (n=8)	Alcohol use disorder (n=15)
Gender (% male), n (%)	3 (37.5)	11 (73.3)
Age (years)	37.5 (24.0–57.0)	44.0 (27.0–61.0)
Weight (kg)	65 (51.0–88.0)	72.0 (49.0–107.5)
BMI (kg/m2)	22.3 (19.8–28.1)	22.4 (18.0–33.9)
Bilirubin (mg/dL)		0.4 (0.2–3.0)
AST (IU/L)		36.0 (14.0–273.0)
ALT (IU/L)		37.0 (14.0–133.0)
Albumin (g/L)		48.0 (32.0–57.5)
INR		0.9 (0.9–1.2)
GGT (IU/L)		120.0 (11.0–3460.0)
ALP (IU/L)		83.0 (41.0–355.0)
CAP		272.0 (208.0–382.0)
FibroScan (Kpa)		6.1 (3.1–72.8)

Median values are represented with range in parentheses for continuous variables or percentage in parentheses for categorical variables. Percentages are calculated based on the number of patients in each group.

ALP, alkaline phosphatase; ALT, alanine aminotransferase; AST, aspartate aminotransferase; AUD, alcohol use disorder; BMI, body mass index; CAP, Controlled attenuation parameter; GGT, gamma-glutamyl transferase; INR, international normalized ratio.

Extended Data Table 2: Liver disease severity in patients with alcohol use disorder (AUD)

Liver disease severity	Alcohol use disorder (n=15)
No liver disease, n (%)	3 (20)
Steatosis, n (%)	5 (33.3)
Steatohepatitis, n (%)	2 (13.3)
Steatofibrosis, n (%)	3 (20)
Unclassified, n (%)	2 (13.3)

Percentages are represented in parentheses.

Extended Data Table 3. Sequences of qPCR primers

Gene	primer	sequence
Mouse *18S*	F	5'–AGTCCCTGCCCTTTGTACACA–3'
	R	5'–CGATCCCAGGGCCTCACTA–3'
Mouse *Chrm4*	F	5'–ATGGCGAACTTCACACCTGTC–3'
	R	5'–CTGTCGCAATGAACACCATCT–3'
Mouse *Cxcl1*	F	5'–TGCACCCAAACCGAAGTC–3'
	R	5'–GTCAGAAGCCAGCGTTCACC–3'
Mouse *Ccl2*	F	5'–ATTGGGATCATCTTGCTGGT–3'
	R	5'–CCTGCTGTTCACAGTTGCC–3'
Mouse *Cxcl5*	F	5'–TGATCCCTGCAGGTCCACA–3'
	R	5'–CTGCGAGTGCATTCCGCTTA–3'
Mouse *Tbp*	F	5'–GTGAAGGGTACAAGGGGGTG–3'
	R	5'–ACATCTCAGCAACCCACACA–3'
Bacteria 16S	F	5'–GTG STG CAY GGY TGT CGT CA–3'
	R	5'–ACG TCR TCC MCA CCT TCC TC–3'

Figures

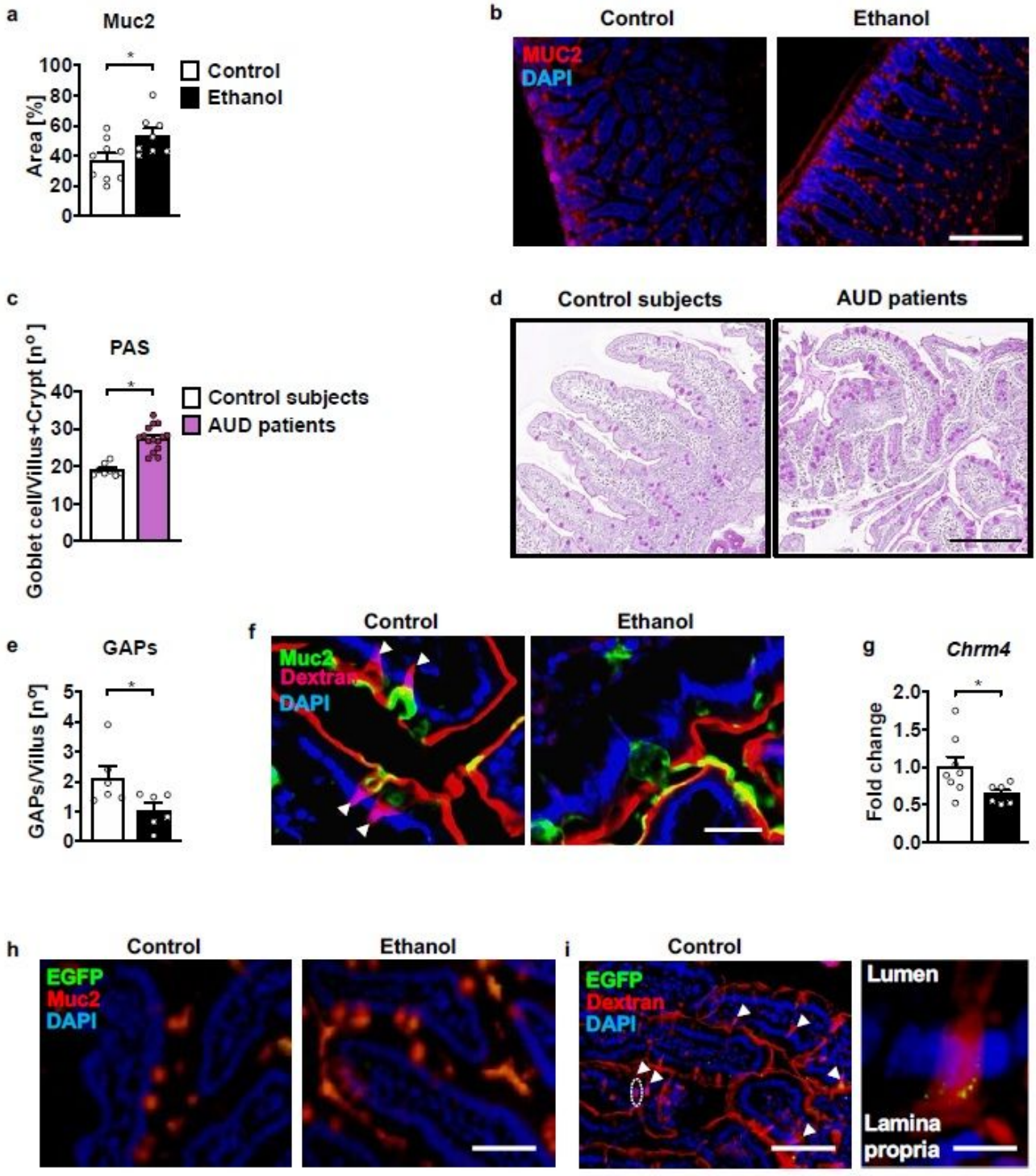

Figure 1

Chronic ethanol alters proximal intestinal GC in mice 344 and humans. (a–b and e–i) C57BL/6 WT mice were fed control (n=6–9) or ethanol containing Lieber DeCarli diets (n=6–8) for 10 weeks. (a) Percentage of Muc2 positive stained area. (b) Representative sections of Muc2 (red) showing GCs and DAPI (blue)

immunofluorescence staining. Scale bar = 250 µm. (c, d) Periodic Acid/Schiff (PAS) staining of paraffin-embedded small intestinal sections of duodenal biopsies from non-alcoholic controls (n=8) and patients with AUD (n=15). (c) Positive cells were enumerated in each villus and crypt. (d) Representative PAS-stained sections showing increased number of GCs in the duodenum of AUD patients as compared with controls. Scale bar = 100 µm. (e) To study GC GAP formation, a 2 cm loop in the small intestine was injected with tetramethylrhodamine (TMR) dextran and GAPs were counted as dextran-filled columns traversing the nucleated epithelium and positive for Muc2 staining. Number of GAPs per villus was quantified. (f) Representative sections stained with TMR-dextran (red) showing GAPs, Muc2 antibody (green) showing GCs and DAPI (blue) marking nuclei. Scale bar = 25 µm. (g) Chrm4 mRNA was quantified by qPCR. (h) E. faecalis genetically modified with an EGFP vector (5 x 109 CFUs) were gavaged 9 h and 1 h before euthanasia (n=6). Representative sections stained with Muc2 antibody (red), EGFP (green) and DAPI (blue). Scale bar = 50 µm. (i) EGFP-E. faecalis (5 x 109 CFUs) were gavaged at 3 and 0.5 h before euthanasia (n=6). Representative section of EGFP (green), TMR-dextran (red) and DAPI (blue) stained intestinal sections. Left panel: scale bar = 100 µm, and right panel (amplification of the white discontinuous oval): scale bar = 12 µm. (f and i) Arrowheads indicate GAPs. P value was determined by two-sided unpaired Student t test or Mann-Whitney U-statistic test. Results are expressed as mean ± s.e.m. *P<0.05.

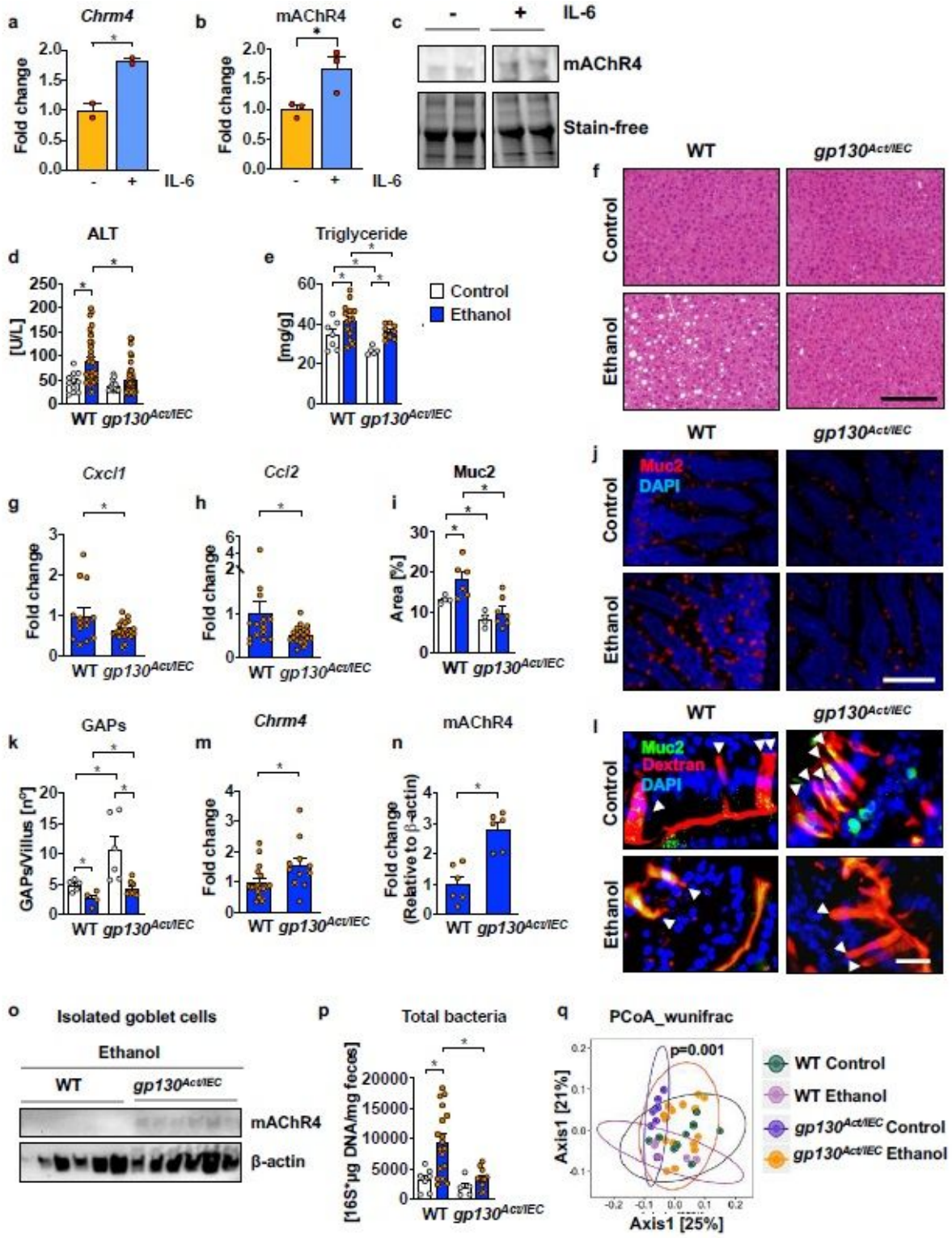

Figure 2

Expression of activated gp130 in IECs prevents ethanol-induced 367 liver disease and promotes GAP formation. (a) Chrm4 mRNA in small intestinal organoids from WT mice (n= 2) was quantitated by qPCR after stimulation with IL-6 (0.02 µg/ml) in the presence of ethanol (10 mM) for 12 h. 6 technical replicates were pooled in each of two independent biological 371 experiments. (b) mAChR4 protein amounts in WT small intestinal organoids after stimulation without (n=3) or with IL-6 (0.5 µg/ml) (n=3) for 24 h. (c)

Representative mAChR4 immunoblots. (d–q) WT mice and gp130Act/IEC littermates were fed control (n=4–15) or ethanol containing Lieber DeCarli diets (n=4–44) for 10 weeks. (d) Plasma levels of ALT. (e) Hepatic triglyceride content. (f) Representative H&E-stained liver sections. Scale bar = 200 µm. (g–h) Hepatic Cxcl1 and Ccl2 mRNAs were quantitated by qPCR. (i) Percentage of Muc2 positive stained area. (j) Representative sections stained with Muc2 antibody (red) showing GCs and DAPI (blue). Scale bar = 200 µm. (k) Number of GAPs per villus. (l) Representative TMR-dextran (red) showing GAPs, Muc2 antibody (green) and DAPI (blue) stained small intestine sections showing GAPs (Arrowheads). Scale bar = 25 µm. (m) Small intestinal Chrm4 mRNA was quantified by qPCR. (n) mAChR4 protein amounts relative to b-actin in isolated GCs. (o) Immunoblots of mAChR4 and b-actin in isolated GCs. (p) Total fecal bacteria were quantitated by qPCR. (q) Principal coordinate analysis (PCoA) with weighted UniFrac of 16S rRNA sequencing of fecal samples. P values were determined by One-way ANOVA with Tukey's post-hoc test (d, e, i, k and p), by two sided unpaired Student t test or Mann-Whitney U-statistic test (a, b, g, h, m and n) and by two sided paired t test. Results are expressed as mean ± s.e.m. *P<0.05.

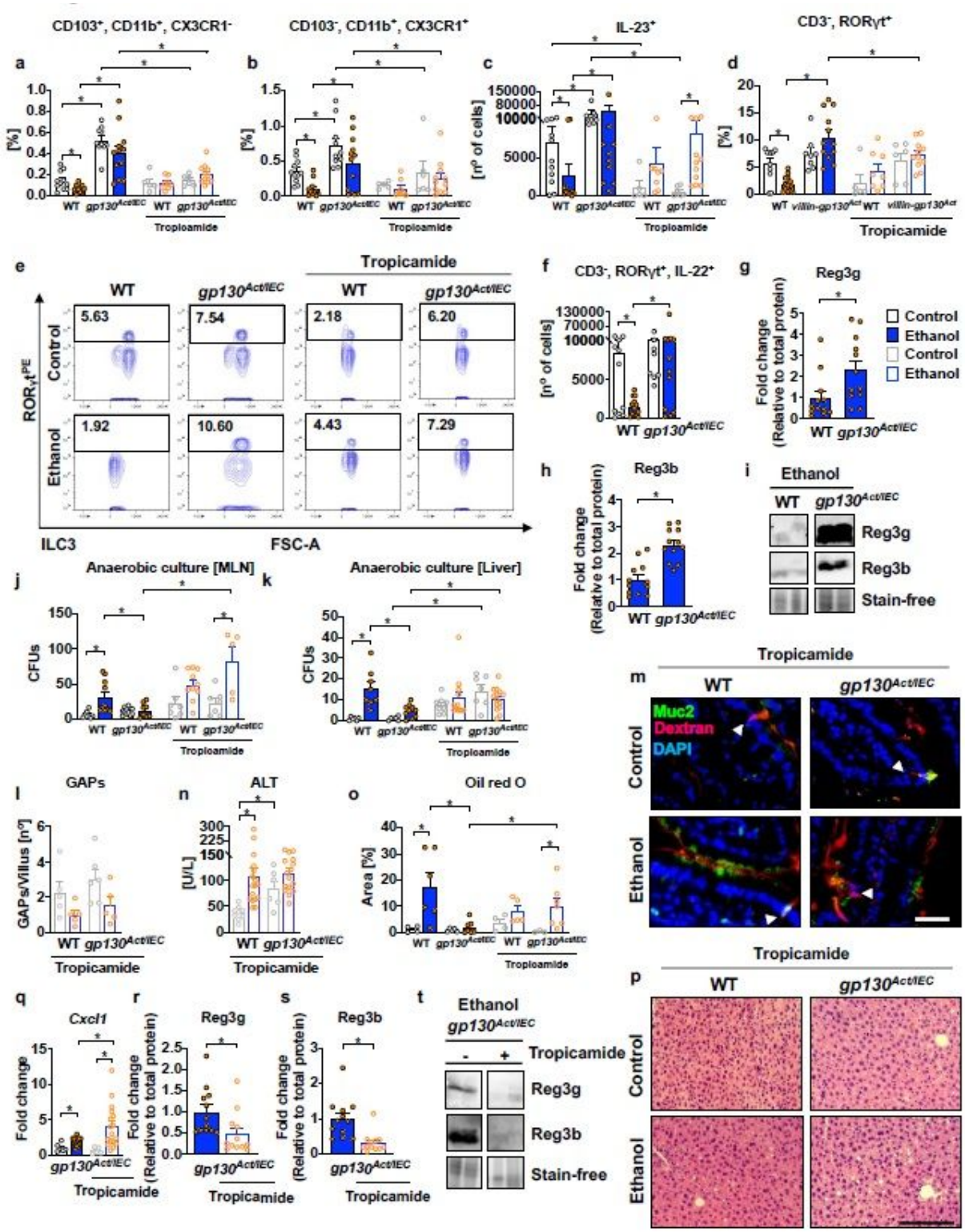

Figure 3

Expression of activated gp130 in IECs stimulates protective 390 intestinal adaptive immune response via mAChR4-mediated GAP formation. (a–t) WT mice and gp130Act/IEC littermates were fed control (n=4–11) or ethanol containing Lieber DeCarli diets (n=6–17) for 10 weeks. (a–d, j–t) A group of littermate mice were treated with the mAChR antagonist tropicamide (20 mg/kg) during the last 29 days (n=5–17). (a–c) Isolated LP immune cells for APC subset identification studies were stimulated with flagellin (100

ng/ml) for 2.5 h. (a–b) Frequencies of tolerogenic APC subsets in total mononuclear phagocyte population were gated according to CD45, MHCII, CD11c, CD103, CD11b, and CX3CR1 expression. (c) Total number of IL-23+ cells in all APCs subsets. (d) Frequencies of ILC3s (CD45+, CD3–, RORγt+) cells after stimulation of isolated LP leukocytes with mouse IL-23 (40 ng/μl) for 4 h. (e) Representative ILC3 and (f) IL-22 expressing ILC3 plots. (g–h) Quantification of Reg3g and Reg3b protein amounts relative to total protein identified by stain-free imaging technology. (i) Representative Reg3g and Reg3b immunoblots. (j, k) Number of colony forming units (CFU) of anaerobically cultured bacteria from sterile collected mesenteric lymph nodes and liver. (l) Number of GAPs per villus. (m) Representative TMR-dextran (red), Muc2 antibody (green) and DAPI (blue) stained small intestinal sections showing GAPs (Arrowheads). Scale bar = 25 μm. (n) Plasma ALT concentrations. (o) Quantification of the Oil red O (ORO)-stained liver sections. (p) Representative H&E stained liver sections. Scale bar = 200 μm. (q) Hepatic Cxcl1 mRNA quantitated by qPCR. (r, s) Reg3g and Reg3b proteins relative to total protein identified by stain-free imaging technology. (t) Representative Reg3g and Reg3b immunoblots. P values were determined by two way (a–d, j–k and o) or one-way ANOVA (f, l, n and q) with Tukey's post-hoc test and by two sided unpaired Student t test or Mann-Whitney U-statistic test (g, h, r and s). Results are expressed as mean ± s.e.m. *P<0.05.

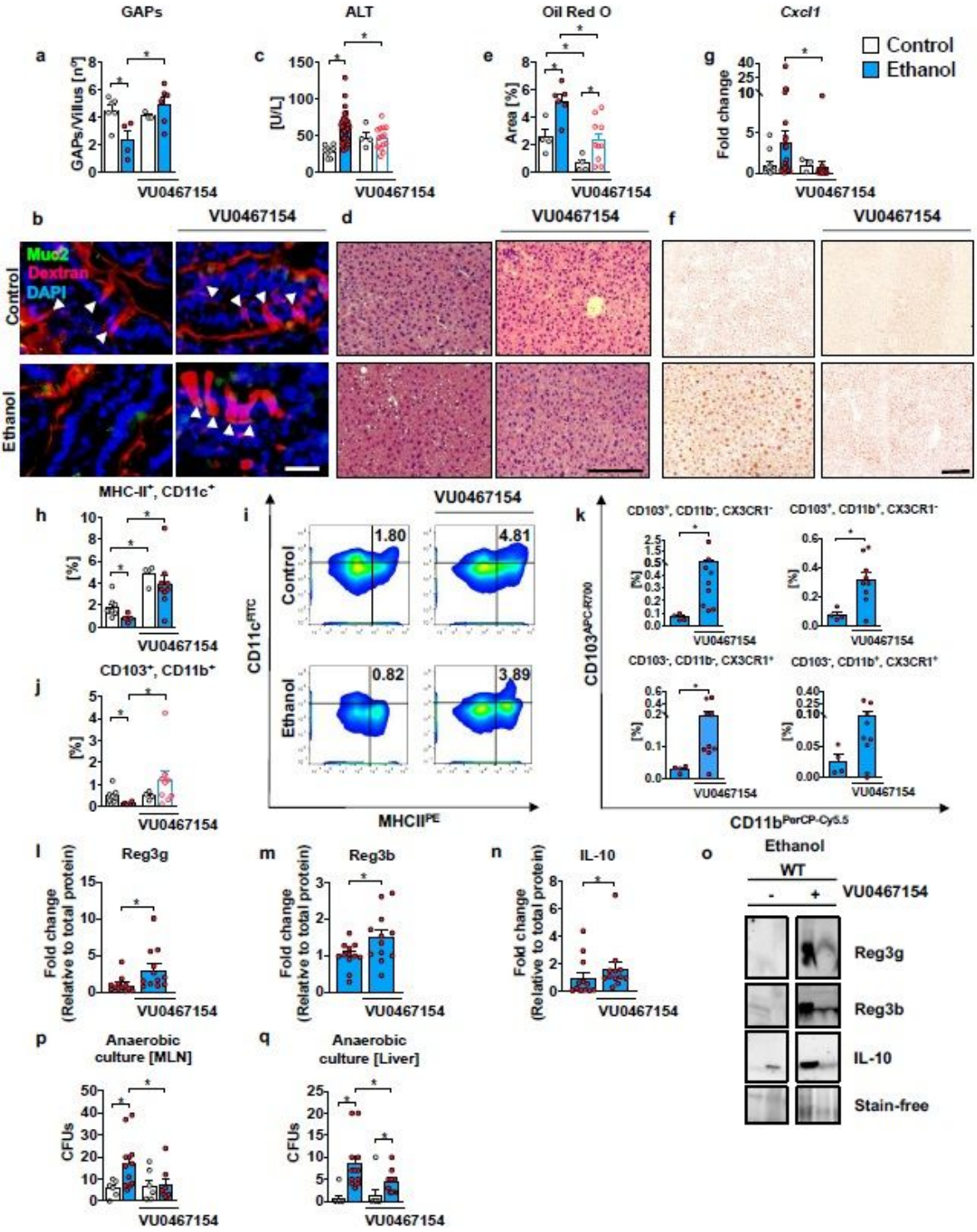

Figure 4

A mAChR4 PAM reduces ethanol-induced liver disease. 413 WT mice were fed control (n=3–9) or ethanol containing Lieber DeCarli diets (n=4–38) for 10 weeks in the presence or absence of the specific mAChR4 PAM VU0467154 (5 mg/Kg), dissolved in the diet during the last 29 days. (a) Number of GAPs per villus. (b) Representative TMR-dextran (red), Muc2 (green) and DAPI (blue) stained small intestine sections showing GAPs (Arrowheads). Scale bar = 25 µm. (c) Plasma ALT concentrations. (d) Representative H&E

stained liver sections. Scale bar = 200 µm. (e) Quantification of ORO-stained liver sections. (f) Representative oil ORO-stained liver sections. Scale bar = 100 µm. (g) Hepatic Cxcl1 mRNA amounts. (h–k) DCs were stimulated with flagellin (100 ng/ml) for 2.5 h before staining. (h) Frequencies of CD45+, MHCII+, CD11c+ APCs in total mononuclear phagocyte population. (i) Representative APCs plots. (j) Frequencies of CD45+, MHCII+, CD11c+, CD103+, CD11b+ DCs. (k) Frequencies of tolerogenic APC subsets according to CD45, MHCII, CD11c, CD103, CD11b and CX3CR1 expression. (l–n) Quantification of Reg3g, Reg3b and IL-10 proteins relative to total protein identified by stain-free imaging technology. (o) Representative Reg3g, Reg3b, and IL-10 immunoblots. (p, q) Number of CFUs of anaerobically cultured bacteria from sterile collected MLNs and liver. P values were determined by one-way ANOVA (a, c, e, g, h, j, p, q) with Tukey's post-hoc test and by two-sided unpaired Student t test or Mann-Whitney U-statistic test (k, l-n). Results are expressed as mean ± s.e.m. *P<0.05.

Supplementary Files

This is a list of supplementary files associated with this preprint. Click to download.

- ExtDataFigGAPsNatureV5.pptx.pdf